

All you need is spin: $SU(2)$ equivariant variational quantum circuits based on spin networks

Richard D. P. East*, Guillermo Alonso-Linaje, and Chae-Yeun Park†

Xanadu, Toronto, ON, M5G 2C8, Canada

September 15, 2023

Abstract

Variational algorithms require architectures that naturally constrain the optimisation space to run efficiently. In geometric quantum machine learning, one achieves this by encoding group structure into parameterised quantum circuits to include the symmetries of a problem as an inductive bias. However, constructing such circuits is challenging as a concrete guiding principle has yet to emerge. In this paper, we propose the use of *spin networks*, a form of directed tensor network invariant under a group transformation, to devise $SU(2)$ equivariant quantum circuit ansätze – circuits possessing spin rotation symmetry. By changing to the basis that block diagonalises $SU(2)$ group action, these networks provide a natural building block for constructing parameterised equivariant quantum circuits. We prove that our construction is mathematically equivalent to other known constructions, such as those based on twirling and generalised permutations, but more direct to implement on quantum hardware. The efficacy of our constructed circuits is tested by solving the ground state problem of $SU(2)$ symmetric Heisenberg models on the one-dimensional triangular lattice and on the Kagome lattice. Our results highlight that our equivariant circuits boost the performance of quantum variational algorithms, indicating broader applicability to other real-world problems.

1 Introduction

Variational algorithms are prominent across physics as well as computer science with particularly fruitful applications in machine learning, condensed matter physics, and quantum chemistry [1, 2, 3, 4]. In such areas, a parameterized function, often called an ansatz, is used to model a probability distribution or a quantum state, and parameters are optimised by minimising a cost function. However, this simple principle does not work without properly chosen ansätze when dealing with a huge parameter space [5]. For this reason, researchers often incorporate an *inductive bias* into their algorithms [6]. An inductive bias is prior knowledge about the system under investigation that can be included in the

*rdp.east@gmail.com

†chae.yeun.park@gmail.com

algorithm to restrict our function classes. Thus the parameterised function favours a better class of outputs for a given target problem. In classical machine learning, for example, it is known that the great success of convolutional neural networks (CNNs) is based on the fact that they contain ‘layers’, essentially parameterised maps, which encode the idea that the content of an image does not change when shifted. Specifically, these convolutional layers are (approximately) translation equivariant: When one shifts the input state by n pixels up and m bits down, the output is also shifted in the same way [7, 8]. Geometric deep learning naturally extends this framework to arbitrary groups [9], suggesting the use of group equivariant layers for learning data with symmetric properties. Neural networks consisting of group equivariant layers have indeed reported better performance for classifying images [7], point clouds [10], and in the modelling of dynamical systems [11]. More broadly they have also been used in a general variational context for tasks such as identifying the ground state of molecules [12].

Recently, the idea of geometric machine learning has been combined with quantum machine learning (QML). Generally speaking, QML algorithms [13] hope to find an advantage over classical algorithms in ML tasks by exploiting the quantum nature of Hilbert space using parameterised quantum circuits. Despite its potential, however, the trainability and generalization performance of QML algorithms without tailored circuit ansätze often scale poorly, limiting their usability for more than tens of qubits [14]. Because of this, recent studies introduced geometric quantum machine learning (GQML) as a guiding principle for constructing a quantum circuit ansatz. The literature shows these symmetry-informed circuits have been successful in offering better trainability and generalization performance [15, 16, 17, 18, 19, 20, 21, 22, 23, 24, 25, 26].

In the GQML setup, the symmetry group $SU(2)$ is particularly interesting as it naturally arises in quantum systems with rotational symmetry. It also corresponds to a natural symmetry of qubits which can be seen as a product of $\text{spin-}\frac{1}{2}$ states. While QML algorithms with the $SU(2)$ symmetry have been previously studied in Refs. [22, 24, 26], implementing the proposed circuit ansätze in quantum hardware was not straightforward. For example, Ref. [24] proposed twirling as a constructive principle for equivariant gates, but computing this twirling formula for a many-qubit gate is highly non-trivial as it involves the summation over the symmetric group (thus over $n!$ terms). In contrast, Ref. [26] showed that a certain form of elements in an algebra generated by the symmetric group (formally written as $\mathbb{C}[S_n]$) can be seen as $SU(2)$ equivariant quantum circuits. Nonetheless, these circuits do not admit a simple decomposition to few-qubit gates (implementable on quantum hardware).

In this paper, we propose an alternative approach to construct $SU(2)$ equivariant circuits. Our circuit ansätze, dubbed *spin-network circuits*, are inspired by spin networks, $SU(2)$ equivariant tensor networks. A core tool for us will be the *Schur* gate (or map, we will use these terms interchangeably) which sends us from a qubit basis to a spin-basis. For example for two qubits, it provides the following mapping $|J=0, J_z=0\rangle = |01\rangle - |10\rangle$, $|J=1, J_z=1\rangle = |00\rangle$, $|J=1, J_z=0\rangle = |01\rangle + |10\rangle$, and $|J=1, J_z=-1\rangle = |11\rangle$ where J is the total angular momentum of two qubits and the J_z is its z -direction component. The advantage of this basis is that it leaves the matrix representations block-diagonal in the total angular momenta [27]. We make use of this by applying certain unitaries to these blocks that allow us to directly parameterise the equivariant maps that make up spin networks. This approach to parameterising equivariant maps via their block decomposition as a QML method coincides directly with what is highlighted in Refs. [28, 22].

Furthermore, we prove that our circuit is mathematically equivalent to other constructions using the representation theory of $SU(2)$. In particular, we prove that both our gates and gates from the twirling formula [22, 24] can be written in the form of generalised permutations as introduced in Refs. [20, 26]. When restricted to unitary operators, all the three constructions give the same set of gates. Our main

theoretical tool is the Schur-Weyl duality which, roughly speaking, posits a duality between $SU(2)$ and the symmetric group S_n . While Refs. [19, 28, 22] already introduced a general theory of equivariant circuits for arbitrary Lie groups, thus presenting a part of our results in a slightly different manner, we develop a theory specifically for the $SU(2)$ group and provide a concrete example using the three-qubit equivariant gate.

We additionally show that the proposed three-qubit gates can be useful for solving a real-world problem with supporting numerical results for $SU(2)$ symmetric models. While our circuits can be used for usual machine learning tasks, e.g., classifying rotationally invariant data, we choose the problem of finding the ground state of $SU(2)$ symmetric Hamiltonians as it provides a better benchmark platform for classically simulated QML models (with ~ 20 qubits). In particular, we solve the Heisenberg model on one-dimensional triangular and Kagome lattices, which have the $SU(2)$ symmetry but are tricky for Monte Carlo based classical algorithms due to the sign problem [29, 30]. We show that our circuit ansätze give accurate ground states with a common parameter optimization technique, which demonstrates the efficiency of our method and justifies the use of our $SU(2)$ equivariant circuits for appropriately symmetric variational and QML problems more generally.

The paper is organised as follows. In Sec. 2, we introduce the preliminaries needed to understand the other sections: The representation theory for $SU(2)$, spin coupling, and spin networks. In Sec. 3, we introduce our ansätze termed *spin-network circuits* which are parameterisable unitary quantum circuits that are also spin networks. To this end the aforementioned Schur gate will be introduced which will be a core technical component in creating our parameterisations. We also concretely present the two and three-qubit unitary *vertex* gates. In Sec. 4, results are presented showing that all $SU(2)$ equivariant unitaries are a form of generalised permutation. This directly connects the work here with that on permutational quantum computing (PQC) [31, 32] and in particular PQC+ as outlined in Ref. [26]. We also discuss the relation with the twirling method introduced in Ref. [24] showing how all $SU(2)$ equivariant gates, i.e., generalised permutations, are the same as the set of all unitary gates generated by twirled Hermitian operators. Next, in Sec. 5, we present the efficacy of the introduced vertex gates by solving the Heisenberg model defined on one-dimensional triangular lattice as well as the two-dimensional Kagome lattice. We then discuss the implications of our results and the connections to the broader literature with a particular focus on PQC+ and loop quantum gravity in Sec. 6 and conclude with a short remark in Sec. 7.

Overall the new contributions of this work are the following: We introduce an $SU(2)$ equivariant quantum circuit ansatz based on spin networks. We provide a number of numerical simulations validating their efficacy; in particular by solving the Heisenberg model on the Kagome lattice. We connect the theory of equivariant operators as seen in the geometric quantum machine learning literature [22] to the work done on PQC+ [20].

2 Preliminaries

Groups and their representation Throughout the paper, we are interested in quantum gates that are equivariant under the $SU(2)$ group transformation. The group $SU(2)$ itself is part of a larger class of groups known as $SU(N)$ is made up of $N \times N$ unitary matrices with a determinant of 1. Formally, we can define an $SU(2)$ equivariant gate as a quantum gate T satisfying

$$U^{\otimes n} T = T U^{\otimes n}, \quad (1)$$

for all $U \in \text{SU}(2)$, where n is the number of qubits in a circuit.

If we consider a circuit C constructed with those gates, thus satisfying $CU^{\otimes n} = U^{\otimes n}C$, one can create an $\text{SU}(2)$ -invariant output state given an $\text{SU}(2)$ -invariant input state. If $|\psi_0\rangle$ is an input state satisfying $|\psi_0\rangle = U^{\otimes n}|\psi_0\rangle$ (we will see an example of such states in Sec. 3), we have

$$U^{\otimes n}C|\psi_0\rangle = CU^{\otimes n}|\psi_0\rangle = C|\psi_0\rangle. \quad (2)$$

Thus such a circuit C can be used for learning tasks involving rotationally invariant data, e.g., finding ground states of Heisenberg spin models or classifying point-sets.

The symmetry we consider here is tightly connected to the notion of groups and their representation. Recall that a group $G = \{g_i\}$ is a set with a map acting on two of its elements $g_1 \cdot g_2 = g_3$ such that there is an identity $e \cdot g = g$, the operations are associative $g_1 \cdot (g_2 \cdot g_3) = (g_1 \cdot g_2) \cdot g_3$, and there is an inverse for all elements $g \cdot g^{-1} = e$. It is also natural to consider an action of a group on a vector. For example, a rotation $R \in \text{SO}(3)$ acts on a three dimensional (real) vector and transforms it. This type of action (on a vector space) is called a *representation* of a group.

Formally speaking, a group representation is a map $R : G \rightarrow \text{GL}(V)$ from the group to the space of invertible linear maps of a vector space V (or equivalently, invertible matrices of dimension N if $\dim(V) = N$) such that $R(g_1 \cdot g_2) = R(g_1) \cdot R(g_2)$. In essence, it is a map from the group to linear maps that preserves the group structure. For a system with a single qubit, a simple map $R(U) = U$ for $U \in \text{SU}(2)$ already defines a representation. One can readily extend this representation to a n -qubit system by defining $\tilde{R}(U) = U^{\otimes n}$, which is also a representation (as $\tilde{R}(U_1 U_2) = (U_1 U_2)^{\otimes n} = U_1^{\otimes n} U_2^{\otimes n} = \tilde{R}(U_1) \tilde{R}(U_2)$). We can then see that to find $\text{SU}(2)$ equivariant gates for an n -qubit system, we have to pay attention to the representation \tilde{R} .

Studying the representation of symmetry introduces the concept of *irreducible representations* (irreps, for short). Firstly, a sub-representation W of V is a subspace $W \leq V$ which satisfies $R(g)W = \{R(g)w : w \in W\} \subseteq W$ for all $g \in G$. Then we say a representation $R : G \rightarrow \text{GL}(V)$ is irreducible if it does not have any non-trivial sub-representations, i.e., if $W \leq V$ and $R(g)W = \{R(g)w : w \in W\} \subseteq W$ for all $g \in G$, then $W = 0$ or $W = V$. Thus by decomposing n -qubit system to vector spaces of different spin numbers (which is always possible by the Peter–Weyl theorem), we may be able to find a structure of equivariant gates. Indeed as we shall see, the *Schur map* sends equivariant operators into a block diagonal form. This form will allow us to explicitly design such maps.

From qubits to spins A spin is an irreducible representation of the $\text{SU}(2)$ group. This vector space is spanned by basis vectors $\{|J, J_z\rangle : -J \leq J_z \leq J\}$ where $2J$ is an integer (e.g., $J = 0$, $J = \frac{1}{2}$, $J = 1$, $J = 3/2$, etc.). Physically J and J_z correspond to the quantised total angular momentum and the angular momentum in the z -direction, respectively (though the z -direction is a convention choice, any would do). For each allowed value of J , we call the corresponding vector space a spin- J system.

A qubit is naturally identified as a spin- $\frac{1}{2}$ particle, by a mapping $|0\rangle = |J = \frac{1}{2}; J_z = \frac{1}{2}\rangle$ and $|1\rangle = |J = \frac{1}{2}; J_z = -\frac{1}{2}\rangle$. When we take two qubits, we are thinking of the basis elements $\{|00\rangle, |01\rangle, |10\rangle, |11\rangle\}$. Consider the angular momentum of two qubits (or two spin- $\frac{1}{2}$ particles, equivalently). It is well known that when one considers two spin-systems of momenta J_1 and J_2 in terms of their joint angular momentum the possible total angular momentum J measurements range from $J = |J_1 - J_2|$ to $J_1 + J_2$. Thus two qubits have the two total angular momentum possibilities of $J = 0$ and $J = 1$. To get the full basis, we must also include the possible J_z values that range from $-J$ to J in steps of 1 [33]. In general, we can

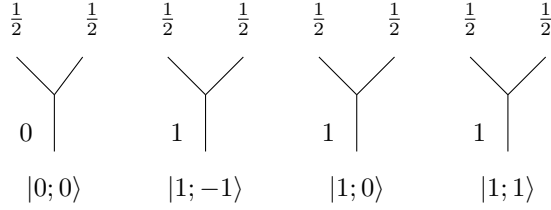


Figure 1: Graphical presentation of the basis constructed by combining angular momentum of two spin- $\frac{1}{2}$ systems and the possible outcomes of total and z -directed angular momenta. These can be seen as two spin networks, corresponding to the two possible total angular momentum values on the bottom edge, with specific $|J; J_z\rangle$ states chosen for the bottom edges Hilbert spaces.

always move from a basis of qubits to a basis of angular momenta by considering pairwise coupling of qubits and subsequent spins, which amounts to considering the possible angular momentum outcomes of a measurement of each pairing. This coupling scheme is depicted in Fig. 1.

For more than two spins, we will have a choice of the order in which we do this. The different orders of pairing the spin-systems amount to different bases (as they correspond to different choices of complete measurements) which we can describe by branching tree-like structures. In Fig. 2 we can see this for three qubits.

In later discussion, we will use $J_{\mathcal{J}} = \mathbb{C}^{2\mathcal{J}+1}$ to denote a spin- \mathcal{J} system. For example, $J_{1/2} = \mathbb{C}^2$ is a vector space for spin- $\frac{1}{2}$ system, i.e., a qubit.

Spin networks We now consider a generalization of equivariant gates using the notion of multi-linear maps. Let us first recall properties of spin-1/2 kets and bras under $g \in \text{SU}(2)$:

$$|a\rangle \xrightarrow{g} g|a\rangle \quad (3)$$

$$\langle b| \xrightarrow{g} \langle b|g^\dagger, \quad (4)$$

where $g = e^{-i\phi\boldsymbol{\sigma}\cdot\hat{n}/2} \in \text{SU}(2)$. Here, $\boldsymbol{\sigma} = \{\sigma_x, \sigma_y, \sigma_z\}$ is a vector of 2×2 Pauli matrices, \hat{n} is a normal vector indicating the direction of the rotation, and ϕ is the angle we rotate.

By identifying kets as vectors and bras as dual vectors, we can generalize the above principle by considering an arbitrary spin- \mathcal{J} system given as $V = J_{\mathcal{J}} = \mathbb{C}^{2\mathcal{J}+1}$. Then $|a\rangle \in V$ and $\langle b| \in V^*$ changes to

$$|a\rangle \xrightarrow{g} R(g)|a\rangle \quad (5)$$

$$\langle b| \xrightarrow{g} \langle b|R(g)^\dagger \quad (6)$$

under the group transformation, where $R(g)$ is a representation of $g \in \text{SU}(2)$. Specifically, it is a $2\mathcal{J}+1$ by $2\mathcal{J}+1$ unitary matrix given by $e^{-i\phi\mathbf{J}\cdot\hat{n}}$ which is a representation of $e^{-i\phi\boldsymbol{\sigma}\cdot\hat{n}/2} = g \in \text{SU}(2)$. Here, $\mathbf{J} = \{J_x, J_y, J_z\}$ is a vector of $2\mathcal{J}+1$ by $2\mathcal{J}+1$ spin matrices satisfying $[J_a, J_b] = i\epsilon_{abc}J_c$ for all $a, b, c \in \{x, y, z\}$ where ϵ_{abc} is the Levi-Civita symbol.

The above principle also induces group transformation formulas for other expressions. For example, one can see that the inner product $\langle a|b\rangle$ is invariant under the group transform as

$$\langle b|a\rangle \xrightarrow{g} \langle b|R(g)^\dagger R(g)|a\rangle = \langle b|a\rangle. \quad (7)$$

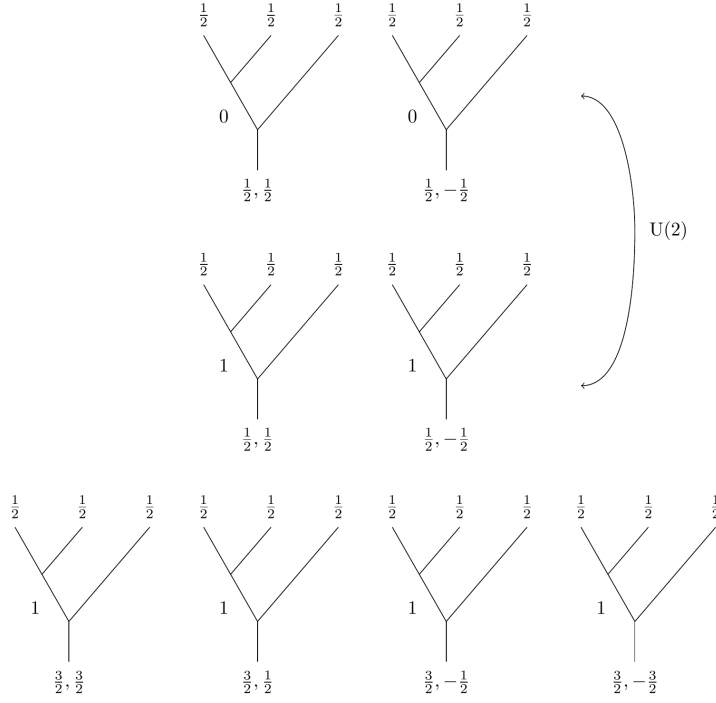


Figure 2: Graphical depiction of a coupling basis of three qubits, where the pairwise coupling of the spaces proceeds from the left (other possibilities give alternative bases). Each row of trees is indexed by the possible total angular momenta that can occur for each composition of two systems. The elements in the rows correspond to the different states these correspond to given a final J_z value on the spaces at the bottom of the trees. Note how the top two rows of diagrams index spaces with the same total angular momentum at the base but that the patterns of coupling that form them are distinct. In Sec. 4, we will see that this allows for the mixing of such states because $SU(2)$ equivariant maps cannot distinguish the two spin coupling structures. Note that in absence of specifying the J_z values the set of diagrams on each row correspond to three separate spin networks as the $SU(2)$ invariance on three-valent networks reduces to spin-coupling rules, this is discussed in more detail in Appendix A.

Note that the last equality is obtained as $R(g)$ is unitary. Next, let us consider a linear map $T : V \rightarrow V$. As T can be written as $T = \sum_{ij} t_{ij} |i\rangle \langle j| \in V \otimes V^*$, we know it changes to

$$T \xrightarrow{g} R(g)TR(g)^\dagger \quad (8)$$

under the transformation.

We now add a constraint that a linear map T also preserves the group structure. In other words, we require T to satisfy

$$R(g)(T|a\rangle) = T(R(g)|a\rangle) \quad (9)$$

for all $g \in G$ and $|a\rangle \in V$, which implies that $R(g)^\dagger TR(g) = T$ (or equivalently, $T = R(g)TR(g)^\dagger$). As $R(g)TR(g)^\dagger$ is nothing but T after the group transformation, a linear map preserving the group

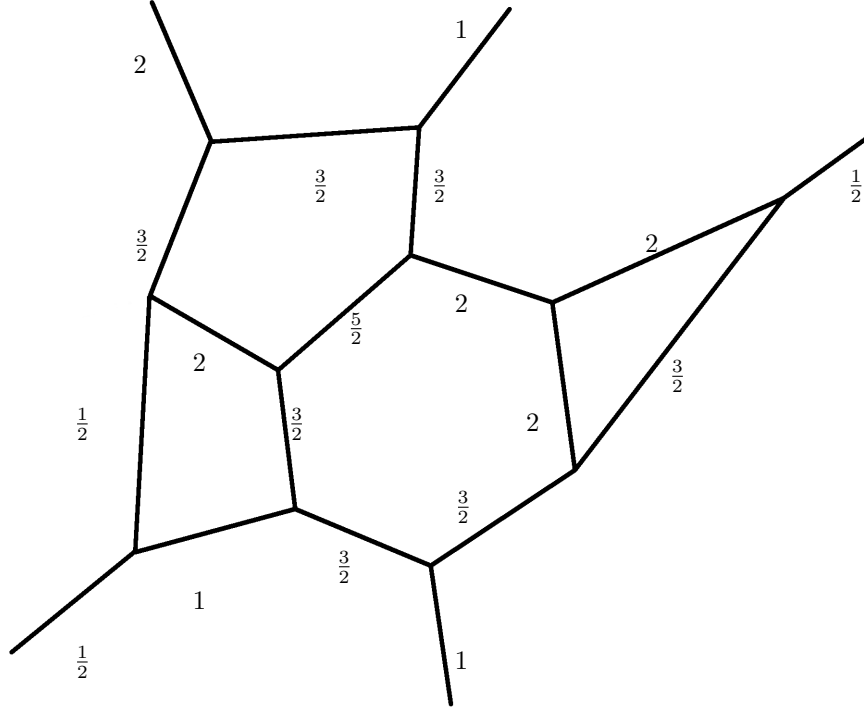


Figure 3: A three valent spin network as typically presented in the broader literature: an edge labelled graph (though directed this is often suppressed in depictions since the spaces are isomorphic). In the three-valent case the edge labels are spins such that around any vertex they meet the Clebsch-Gordan conditions $j_1 + j_2 + j_3 \in \mathbb{N}$ and $|j_1 - j_2| \leq j_3 \leq j_1 + j_2$, which can be shown to exactly match when the vertex is an invariant subspace of $SU(2)$ (See Appendix A for more details).

structure is a matrix that is invariant under the group transformation (given by conjugation with $R(g)$).

One may further extend this property to multilinear maps (tensors). For example, a two-qubit gate is a linear map T between $V^{\otimes 2}$ and $V^{\otimes 2}$ (where $V = J_{1/2} = \mathbb{C}^2$ in the standard formulation). If we add the equivariant condition to this gate, i.e., $R(g)^{\otimes 2}T = TR(g)^{\otimes 2}$, this is nothing but the condition for a group-structure preserving map. As a two-qubit gate T can be considered as an element of $V^{\otimes 2} \otimes (V^*)^{\otimes 2}$, T becomes

$$T \xrightarrow{g} R(g)^{\otimes 2}T(R(g)^\dagger)^{\otimes 2} = T, \quad (10)$$

under the group transformation, where the last equality is from the equivariant condition. Thus there is one-to-one correspondence between group-structure preserving maps and group-invariant tensors¹. In

¹Formally, the set of these tensors is written as $\text{Inv}_{SU(2)}(V^{\otimes n} \otimes (V^*)^{\otimes m})$.

other words, if we consider a general (possibly non-unitary) linear map between $V^{\otimes n}$ and $V^{\otimes m}$ (where n and m can be different integers) preserving the group structure, it can be seen as a group-invariant tensor with n input legs and m output legs [34, 35] (often called a tensor of type (n, m)).

Now we consider a tensor network which consists of $SU(2)$ invariant tensors with contraction edges that run over irreps of $SU(2)$. This special type of network is called a “spin network”; an example from the broader literature can be seen in Fig. 3. These were originally introduced by Penrose [36] in the very different context of a combinatorial derivation of space-time. In modern physics, they are typically discussed as the basis of quantised space in the covariant formulation of loop quantum gravity [37] (though not the focus of this work, interested readers can look Appendix C for the connection). Roughly, a spin network is a directed graph where each edge has an associated spin and each vertex v has an associated equivariant map from the tensor product of the incoming spins to the tensor product of the outgoing spins. Formally, we describe this as a graph detailing the connectivity of vertices v with incoming edges e_{in} and outgoing ones e_{out} such that for every vertex, there is an associated map T_v such that $T_v \in \bigotimes_{i \in e_{in}} \bigotimes_{o \in e_{out}} J_{j_i} \otimes J_{j_o}^*$, where J_{j_i} and J_{j_o} are the incoming and outgoing respective Hilbert spaces. We further require T_v to satisfy the equivariant condition

$$\bigotimes_{i \in e_{in}} \bigotimes_{o \in e_{out}} T_v (R_{j_i}(g) J_{j_i} \otimes J_{j_o}) = \bigotimes_{i \in e_{in}} \bigotimes_{o \in e_{out}} T_v (J_{j_i} \otimes R_{j_o}(g) J_{j_o}) \quad \forall g \in G, \quad \forall v, \quad (11)$$

where $R_{j_i}(g)$ and $R_{j_o}(g)$ are the representations of the group element g acting on the J_{j_i} and J_{j_o} , respectively. From the discussion above, each map associated with a vertex (T_v) can be regarded as a group-invariant tensor. In this way, spin networks are a form of tensor network where the composing tensors are elements in the invariant sub-spaces of a group and the contraction is over spin-spaces of size $2J + 1$. For a more detailed description of these objects, we direct the reader to Appendix A. For our interests, it is sufficient to say that we can build a quantum circuit that is inherently $SU(2)$ equivariant by restricting to specific spin networks whose vertices can be interpreted as parameterised qubit unitaries.

Within the literature, spin networks that form binary trees have been particularly prominent. The simplest example is of the kind seen in Fig. 1 where we ignore the specification of the J_z state at the bottom and focus only on the total angular momentum (so there are just two unique diagrams from this perspective). A more general example is provided by Fig. 2 where we have three spin-spaces coming together which naturally leads to three possible spin networks, specifically one for each row. The reason the columns are not different networks is because they amount to fixing a choice of J_z value on one edge, which is a choice of contraction index (i.e., final projection). Thus such a fixing does not alter the spin-spaces in the definition of the network². It should be noted that spin networks have previously been considered in the broader quantum information literature as diagrammatic qubit maps and as variational maps for numerical investigations of LQG on quantum computers Refs. [38, 39, 40, 41] though never as general $SU(2)$ equivariant variational ansätze.

²The careful reader might note that here we are simultaneously looking at diagrams that correspond to the rules of angular momentum addition and saying these match to the definition of the vertices being $SU(2)$ invariant sub-spaces. The connection is outlined in Appendix C where we see that the invariant spaces can be decomposed in terms of Clebsch-Gordan coefficients which are the exact same elements used in deriving angular momentum decompositions.

3 Spin-network circuits

In this section, we outline circuit ansätze designed based on the principles of spin networks. To show their utility, we present concrete examples which in turn are used for our simulations further below in Sec. 5. Due to the circuits' mathematical equivalence to certain types of spin network, they are explicitly $SU(2)$ equivariant. While the core ideas are outlined here, we discuss the finer points, related concepts, and generalisations in Appendix A.

Our circuits, termed *spin-network circuits*, are a specific form of spin network. They are spin networks where all vertices have an even number of external wires, and every wire in the network is spin- $\frac{1}{2}$, and so are formed of qubits. Among all external wires for each vertex, half are inputs, and the other half are outputs; the combination of these vertices amounts to a quantum circuit. For this reason, when viewed as a quantum circuit, we refer to the vertices as *vertex gates*. Critically, the vertices of a spin network are equivariant maps between the input and output edges, which is a direct consequence of the definition given in Eq. (11). This means the resultant circuit is also equivariant. An important property of spin networks with vertices with more than three edges is that they can be parameterised (see Appendix A). By training over these parameters we thus arrive at a trainable equivariant network.

Schur gate and two qubit vertex gate The simplest spin-network circuit is built from vertex gates acting solely on two qubits. To understand the structure of this gate, and its later generalisations, we first require the two-qubit Schur gate as a prerequisite [42]:

$$S_2 = \begin{pmatrix} 1 & 0 & 0 & 0 \\ 0 & \frac{1}{\sqrt{2}} & \frac{1}{\sqrt{2}} & 0 \\ 0 & 0 & 0 & 1 \\ 0 & \frac{1}{\sqrt{2}} & -\frac{1}{\sqrt{2}} & 0 \end{pmatrix} \quad (12)$$

This gate is a unitary operator that maps the computational basis of two qubits to the spin-basis of their combined J and J_z angular momenta. As qubits can be seen as spin- $\frac{1}{2}$ spaces, with spin-up and spin-down being assigned to 0 and 1 respectively, then qubit registers correspond to tensor products of spin- $\frac{1}{2}$ irreps. While these are individually irreducible, their product is not and so can be block diagonalised into irreducible components. In the case of two qubits, it is often typical to write that $J_{\frac{1}{2}} \otimes J_{\frac{1}{2}} \simeq J_0 \oplus J_1$ which says that a tensor product of two spin- $\frac{1}{2}$ spaces is isomorphic to the direct sum of a spin-0 and a spin-1 space telling us that there is a unitary map between them. The two qubit Schur gate performs exactly this map. Looking at this in terms of the computational basis, the two qubit Schur gate maps the computational basis states to the following basis (where we often drop the normalisation in later exposition): $|J = 1, J_z = 1\rangle = |00\rangle$, $|J = 1, J_z = 0\rangle = \frac{1}{\sqrt{2}}(|01\rangle + |10\rangle)$, $|J = 1, J_z = -1\rangle = |11\rangle$, and $|J = 0, J_z = 0\rangle = \frac{1}{\sqrt{2}}(|01\rangle - |10\rangle)$, which is occasionally referred to as the triplet/singlet basis³. In general, though trivially in the two-qubit case, we can say that the two-qubit Schur map sends us to the sequentially coupled basis of two qubits exactly as depicted in Fig. 1. As was discussed in Sec. 2 above, this amounts to two different binary spin networks with the J_z values specified on the base as first outlined in Ref. [43].

The two-qubit Schur gate from Eq. (12) is the simplest Schur map that sends us from the tensor product of qubits to the direct sum of spins. Precisely, the general form of the Schur map follows the

³For reasons of the different total angular momentum states energies separating under the presence of an external magnetic field.

prescription:

$$S_n : J_{\frac{1}{2}}^{\otimes n} \rightarrow \bigoplus_k J_k \quad (13)$$

where we understand $J_{\frac{1}{2}}^{\otimes n}$ as the Hilbert space corresponding to n qubits and k ranges over the irreducible representations of $SU(2)$ that make up the space in the spin-basis where we note that *irreps can repeat, in which case we say there is a multiplicity*⁴.

The matrix elements of the Schur map can be obtained by using *Clebsch-Gordan coefficients* and coupling paths of qubits. Each Clebsch-Gordan coefficient $\langle j_1 m_1 j_2 m_2 | JM \rangle = c_{j_1 m_1 j_2 m_2}^{JM}$ corresponds to the projection of two particular spin-states into their combined angular momenta. Thus its matrix entries correspond to the Clebsch-Gordan coefficients that result from projecting coupled spin systems (specifically one spin- $\frac{1}{2}$ qubit with whatever angular momentum has been reached by previous spin-couplings) into a particular total J value. Each coefficient that gets multiplied corresponds to a vertex in the coupling diagrams that index each of the spin-basis elements (such as those seen in Fig. 2), i.e., each element of the Schur map can be obtained by multiplying the Clebsch-Gordan coefficients associated with each vertex of the spin-coupling diagram.

As an example, let us consider the three-qubit case. Here each element in the matrix of the Schur map corresponds to $c_{j_1, m_1; j_2, m_2}^{j', m'} c_{j', m'; j_3, m_3}^{J, M}$ for some choice of $j' \in \{0, 1\}$ and $-j' \leq m' \leq j'$. Here j' stands for the resulting spin from coupling the first two qubits, which leads to possible total spin momenta $j' = 0$ and $j' = 1$. In the following, we focus on the spin-0 case ($j' = 0$). This corresponds to the coefficient $c_{\frac{1}{2}, m_1; \frac{1}{2}, m_2}^{0, 0}$. When we in turn couple with the third qubit the only possible outcome for the total angular momentum is $\frac{1}{2}$, so the combined coupling coefficient for these total angular momenta is $c_{\frac{1}{2}, m_1; \frac{1}{2}, m_2}^{0, 0} c_{\frac{1}{2}, m_1; 0, 0}^{\frac{1}{2}, m}$. These choices single out a particular recoupling path with associated final J_z values on the root (as seen in Fig. 1) and so a row in the matrix. The computational basis, equivalently the J_z values for the individual qubits, fixes the columns (for more on this see Ref. [44]). For practical implementations, it is important to note that the Schur gate can be implemented in polynomial time and the literature already contains examples of specific methods to do this [44, 45].

In the case of two qubits there is only a single coefficient to consider in each element of the matrix and so we have the following:

$$S_2 = \begin{pmatrix} c_{\frac{1}{2}, \frac{1}{2}; \frac{1}{2}, \frac{1}{2}}^{1, 1} & c_{\frac{1}{2}, \frac{1}{2}; \frac{1}{2}, -\frac{1}{2}}^{1, 1} & c_{\frac{1}{2}, -\frac{1}{2}; \frac{1}{2}, \frac{1}{2}}^{1, 1} & c_{\frac{1}{2}, -\frac{1}{2}; \frac{1}{2}, -\frac{1}{2}}^{1, 1} \\ c_{\frac{1}{2}, 0; \frac{1}{2}, \frac{1}{2}}^{1, 0} & c_{\frac{1}{2}, 0; \frac{1}{2}, -\frac{1}{2}}^{1, 0} & c_{\frac{1}{2}, -\frac{1}{2}; \frac{1}{2}, \frac{1}{2}}^{1, 0} & c_{\frac{1}{2}, -\frac{1}{2}; \frac{1}{2}, -\frac{1}{2}}^{1, 0} \\ c_{\frac{1}{2}, -\frac{1}{2}; \frac{1}{2}, \frac{1}{2}}^{1, -1} & c_{\frac{1}{2}, -\frac{1}{2}; \frac{1}{2}, -\frac{1}{2}}^{1, -1} & c_{\frac{1}{2}, \frac{1}{2}; \frac{1}{2}, \frac{1}{2}}^{1, -1} & c_{\frac{1}{2}, \frac{1}{2}; \frac{1}{2}, -\frac{1}{2}}^{1, -1} \\ c_{\frac{1}{2}, 0; \frac{1}{2}, \frac{1}{2}}^{0, 0} & c_{\frac{1}{2}, 0; \frac{1}{2}, -\frac{1}{2}}^{0, 0} & c_{\frac{1}{2}, -\frac{1}{2}; \frac{1}{2}, \frac{1}{2}}^{0, 0} & c_{\frac{1}{2}, -\frac{1}{2}; \frac{1}{2}, -\frac{1}{2}}^{0, 0} \\ c_{\frac{1}{2}, \frac{1}{2}; \frac{1}{2}, \frac{1}{2}}^{0, 1} & c_{\frac{1}{2}, \frac{1}{2}; \frac{1}{2}, -\frac{1}{2}}^{0, 1} & c_{\frac{1}{2}, -\frac{1}{2}; \frac{1}{2}, \frac{1}{2}}^{0, 1} & c_{\frac{1}{2}, -\frac{1}{2}; \frac{1}{2}, -\frac{1}{2}}^{0, 1} \end{pmatrix} = \begin{pmatrix} 1 & 0 & 0 & 0 \\ 0 & \frac{1}{\sqrt{2}} & \frac{1}{\sqrt{2}} & 0 \\ 0 & 0 & 0 & 1 \\ 0 & \frac{1}{\sqrt{2}} & -\frac{1}{\sqrt{2}} & 0 \end{pmatrix}$$

which indeed matches the definition of the two qubit Schur gate in Eq. (12).

Once we are in the spin basis, we can elegantly construct the two-qubit vertex gate by applying a phase solely on the spin-0, or singlet, element $|J = 0, J_z = 0\rangle$ (see Lemma 1 below). Intuitively if a map is $SU(2)$ equivariant, so that you can isolate and apply group representations before or after the map, then the different spin-irreps should not interact under the mapping and remain differentiated – as matrices this is why the map is block diagonal in the spin basis. For the two-qubit case, up to a

⁴More formally the Schur map implements the isomorphism given in Theorem 2 below.

$$\begin{aligned}
V(\theta) \in \text{Inv}_{\text{SU}(2)}(J_{\frac{1}{2}} \otimes J_{\frac{1}{2}} \otimes J_{\frac{1}{2}} \otimes J_{\frac{1}{2}}) &= |J=1\rangle\langle J=1| \oplus e^{i\theta} |J=0\rangle\langle J=0| \\
&= \text{Diagram with } J=1 \text{ label} \oplus e^{i\theta} \text{Diagram with } J=0 \text{ label}
\end{aligned}$$

Figure 4: Depiction of a parameterised gate $V(\theta) \in \text{Inv}_{\text{SU}(2)}(J_{\frac{1}{2}} \otimes J_{\frac{1}{2}} \otimes J_{\frac{1}{2}} \otimes J_{\frac{1}{2}})$ living in the basis block diagonal in the space of $\text{SU}(2)$ equivariant unitaries on two qubits and therefore a four-valent spin network vertex. We can see it is composed of a superposition of two three-valent spin networks indexed by the possible internal spin-0 or spin-1 edge (see Appendix C for details on spin network decompositions). On the right hand side we allude to the geometric interpretation of the basis where the couplings correspond to triangles of different quantised edge length (again see Appendix C).

global phase, this amounts to just a phase on one of the spaces:

$$P_2(\theta) = \left(\begin{array}{ccc|c} & & & 0 \\ & \mathbb{1}_3 & & 0 \\ 0 & 0 & 0 & e^{i\theta} \end{array} \right) \quad (14)$$

In terms of spin networks, which we recall are equivariant maps, the Schur gate is sending us to the two possible coupling options. Two qubits coupling to spin-0 or to spin-1. In isolation⁵, these correspond to two possible spin networks. The parameterised gate $P_2(\theta)$, applies a phase on the spin-0 network. In Sec. 4, we will see this structure completely characterises the possible unitary equivariant maps. To understand how this phase manages to isolate only one part of the spin space, we need to look again at representations. The spin-basis is always such that any group representation in this basis (up to row permutation depending on your exact basis choices and Schur gate, which can vary a little in the literature) is block diagonal. Each individual block is associated to a particular total angular momentum J and a way of arriving at it by sequentially coupling spin-1/2s as seen in Fig. 2. In this way, given a tensor product of n -spins, each block corresponds to one of the $2J + 1$ dimensional spin spaces of its direct product decomposition as seen in Eq.(13). As we now know, for the case of two qubits, we either have spin-0 or spin-1 and so this block decomposition resembles the following:

$$\left(\begin{array}{ccc|c} & & & 0 \\ \text{spin-1} & & & 0 \\ & & & 0 \\ 0 & 0 & 0 & \text{spin-0} \end{array} \right) \quad (15)$$

The block diagonal structure is critical for our $\text{SU}(2)$ equivariant ansätze. As we will see below, their general structure is to apply parameterised maps that act independently on blocks of different sizes (which are different irreducible representations) and as unitaries that mix those parts of repeated blocks of the same irreducible representation when they correspond to the same J_z value. Indeed this structure completely characterises equivariant maps, as is shown below in Sec. 4. As such we can create an equivariant ansatz for $\text{SU}(2)$, i.e., spin rotation symmetry. We note it bears some resemblance with work seen in Ref. [22].

⁵An equivariant gate acting on two or more qubits can be regarded as a spin network with more than three legs. One can specify intermediate vertex choices for such a network, which introduces a sub-network structures.

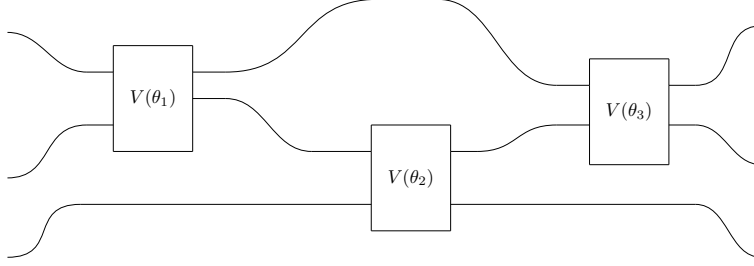


Figure 5: A four-valent spin-network circuit that can be trained over the free parameters in its vertex gates. The curved qubit wires serve only to highlight the idea that such spin-network circuits are both spin networks and quantum circuits.

This leads us to the definition of a vertex gate.

Definition 1. *The two qubit vertex gate $V_2(\theta)$ is composed as follows:*

$$\boxed{V_2(\theta)} = \boxed{S_2} \boxed{P_2(\theta)} \boxed{S_2^\dagger}$$

where S_2 is the two qubit Schur gate and $P_2(\theta)$ is the controlled phase seen in Eq. (14).

What we have created is specific two-qubit gates that live in the space of equivariant maps from, and to, the tensor product of two spin- $\frac{1}{2}$ s, these can be seen depicted in Fig. 4. These, by definition, are elements of the vertices of a four-valent spin network with edges fixed as qubits. We can see the spin network as corresponding to an operator formed by sequential gate operations as seen in Fig. 5

Three and more qubit vertex gates Every even valence spin network vertex admits a possible vertex gate (though 2 is trivial; see Appendix C). A second, more subtle, example is the three-qubit Schur gate S_3 .

$$S_3 = (c_{j_1, m_1; j_2, m_2}^{j_4, m_4} c_{j_4, m_4; j_3, m_3}^{J, M}) = \begin{pmatrix} 1 & 0 & 0 & 0 & 0 & 0 & 0 & 0 \\ 0 & \frac{1}{\sqrt{3}} & \frac{1}{\sqrt{3}} & 0 & \frac{1}{\sqrt{3}} & 0 & 0 & 0 \\ 0 & 0 & 0 & \frac{1}{\sqrt{3}} & 0 & \frac{1}{\sqrt{3}} & \frac{1}{\sqrt{3}} & 0 \\ 0 & 0 & 0 & 0 & 0 & 0 & 0 & 1 \\ 0 & \sqrt{\frac{2}{3}} & -\frac{1}{\sqrt{6}} & 0 & -\frac{1}{\sqrt{6}} & 0 & 0 & 0 \\ 0 & 0 & 0 & \frac{1}{\sqrt{6}} & 0 & \frac{1}{\sqrt{6}} & -\sqrt{\frac{2}{3}} & 0 \\ 0 & 0 & \frac{1}{\sqrt{2}} & 0 & \frac{1}{\sqrt{2}} & 0 & 0 & 0 \\ 0 & 0 & 0 & -\frac{1}{\sqrt{2}} & 0 & \frac{1}{\sqrt{2}} & 0 & 0 \end{pmatrix} \quad (16)$$

Again we have a parameterised $P_3(\vec{\theta})$ rotation applied in the spin basis. In the parameterised gate we define a three-qubit unitary that acts on the two spin- $\frac{1}{2}$ spaces that come from the block diagonal decomposition of three qubits $J_{\frac{1}{2}} \otimes J_{\frac{1}{2}} \otimes J_{\frac{1}{2}} \simeq J_{\frac{3}{2}} \oplus J_{\frac{1}{2}} \oplus J_{\frac{1}{2}}$. The difference between this gate and the

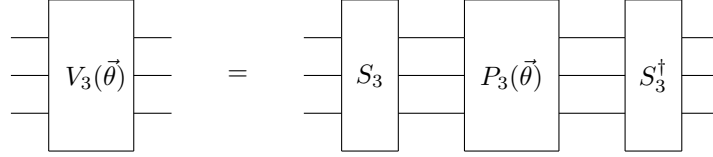
one above is that the above two-qubit vertex gate lacks multiplicities, i.e., multiple blocks of the same size, meaning the only option is to have a phase on each different block. If we have multiple blocks of the same size this indicates that there are multiple sub-spaces of the state space with the same total angular momentum and that multiple states exist with same quantum numbers $|J; J_z\rangle$. In terms of $SU(2)$ equivariant maps, these are states that we can interchange without altering the structure of the space – this implies that our vertex gates are not just phases on differing blocks but also unitaries that mix the multiple copies of $|J; J_z\rangle$ (see Fig. 2 for how our unitaries act on this space and Sec. 4 for theoretical backgrounds). As an example, for our three qubit space we have one spin- $\frac{3}{2}$ space and two spin- $\frac{1}{2}$ spaces so it suffices to have a single unitary acting to mix the two $|\frac{1}{2}, J_z\rangle$ states. The general matrix has the following form:

$$P_3(\vec{\theta}) = \left(\begin{array}{c|c} \mathbb{1}_4 & 0_4 \\ \hline 0_4 & U_2(\vec{\theta}) \otimes \mathbb{1}_2 \end{array} \right) = \left(\begin{array}{c|c} \mathbb{1}_2 & 0_2 \\ \hline 0_2 & U_2(\vec{\theta}) \end{array} \right) \otimes \mathbb{1}_2 \quad (17)$$

where $U_2(\vec{\theta})$ is a unitary matrix of dimension two, implying this gate has four real parameters. One might imagine that there could be a relative phase here on the isolated spin- $\frac{3}{2}$ space but (up to a global phase) this is a sub-case of the unitary acting on the two spin- $\frac{1}{2}$ components. We note that this gate can be written as the **ControlledUnitary** gate between the first and second qubits (and acting trivially on the third qubit), where the **ControlledUnitary** is generated by $\{|1\rangle\langle 1| \otimes \mathbb{1}_2, |1\rangle\langle 1| \otimes X, |1\rangle\langle 1| \otimes Y, |1\rangle\langle 1| \otimes Z\}$.

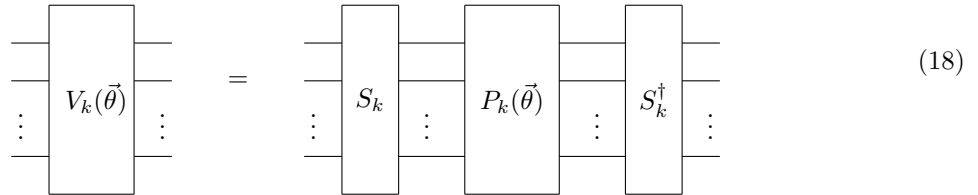
This leads to the three qubit vertex gate definition.

Definition 2. *The three qubit vertex gate is composed as follows:*



where S_3 is the three qubit Schur gate and $P_3(\vec{\theta})$ is the controlled unitary seen in Eq. (17).

Our construction extends to arbitrary k -qubit gates. In general these spin-network circuits have the following shape:



Here, $\vec{\theta}$ is the vector of trainable parameters. These are the free variables needed to parameterise the space of the l different irreps that make up the spin basis of k qubits $\oplus_{i=1}^l (U_i \otimes \mathbb{1}_{d_i})$ where each $U_i \in U(m_i)$ is a unitary of the size of the multiplicity of the i^{th} representation and d_i is the dimension of the i^{th} irrep (i.e., $2J + 1$ where J is the spin number of the subspace). These unitaries specifically act to mix the states with the same J_z value between the repeated irreps (again see Sec. 4). As any

arbitrary k -qubit gate can be decomposed into $\mathcal{O}(k)$ elementary gates [46], one can implement a spin-network circuit with a given parameter $\vec{\theta}$ using quantum hardware with a constant overhead (as k is constant). However, it is generally difficult to decompose a spin-network circuit with arbitrary $\vec{\theta}$ to single and two-qubit parameterised quantum gates with a fixed structure and so this is a compilation task that requires further study (i.e., finding a circuit with single and two-qubit parameterised gates that generate the equivariant gate).

An interesting question is how the few-qubit gates introduced in this section act on the global $SU(2)$ subspace. For example, let us consider a spin-3 irreducible subspace of 8 qubits (e.g., a state $\cos(\theta)|11111110\rangle + \sin(\theta)|11011111\rangle$ lives in this subspace). How can we write down the matrix form of the gate in this subspace? In the following section we answer this question by outlining the theory of $SU(2)$ equivariant gates from a global perspective. Interestingly, we will show that all $SU(2)$ equivariant gates are the generalised permutations introduced in Ref. [20].

4 Equivariant gates from representation theory

In the previous section, we have introduced the Schur map for constructing gates that commute with the $SU(2)$ group action. However, the transformed basis from the Schur map only block diagonalise $SU(2)$ action, and an additional parameterised unitary gate (introduced as $P(\theta)$) acting between the blocks was necessary to build an equivariant gate. In this section, we completely characterise all possible forms of such unitary gates by developing a general theory of $SU(2)$ equivariant operations. Furthermore, using the representation theory of $SU(2)$ and the duality between the permutation group S_n and $SU(2)$, we prove that $SU(2)$ equivariant operations are generalised permutations (which we formally define below), and conversely, all generalised permutations are also equivariant operators. Using this result, we prove that our construction of equivariant gates gives the identical set of gates from the twirling formula and parameterised permutations introduced in Refs. [20, 24]. We further answer the question raised at the end of the previous section using this identification. As this section is rather technical and not directly related to simulation results, the readers may directly jump to later sections.

4.1 Equivariant operations as the center of a representation

Let us start with the definition of the commutant algebra.

Definition 3. For a given representation $R : T \rightarrow GL(\mathbb{C}^n)$, we define the commutant algebra $C(R)$ as

$$C(R) = \{T \in \mathcal{M}_n(\mathbb{C}) : TR(g) = R(g)T \text{ for all } g \in G\}, \quad (19)$$

where $\mathcal{M}_n(\mathbb{C})$ is the set of $n \times n$ complex matrices.

One can verify that $C(R)$ indeed forms an algebra (under matrix addition and multiplication). This tells us that equivariant gates for $U^{\otimes N}$ with $U \in SU(2)$ are nothing but unitary operators in $C(U^{\otimes N})$.

Throughout the rest of this subsection, we will construct a complete set of equivariant gates. To achieve this, it will be practical to pay closer attention to the structure of the commutant algebra. To this end we consider the following lemmas.

Lemma 1 (Schur's lemma). *A homomorphism preserving the group structure $f \in \text{Hom}_G(V, W)$ is a homomorphism satisfying $f(gv) = gf(v)$ for all $g \in G$ and $v \in V$. If V and W are two irreducible representations of a group G over \mathbb{C} , then f must be $c\mathbb{1}$ for $c \in \mathbb{C}$ or 0.*

In short, a structure-preserving map between two irreps is either proportional to the identity (which implies that the vector space V and W are essentially the same) or zero (they are different irreps). A proof can be found in Refs. [47, 33]. As $T \in \text{Hom}_G(V, W)$ in Definition 3 is a linear map, the condition $TR(g) = R(g)T$ can be written in terms of matrices. From this we can more easily construct the commutant algebra for some simple cases, showing for example that the commutant of a direct sum of differing irreps is a direct sum of two scaled identity maps.

Lemma 2. *Let $R^{(1)}$ and $R^{(2)}$ be different irreducible representations of a group G with dimensions d_1 and d_2 , respectively. Let us consider a representation $R = R^{(1)} \oplus R^{(2)}$, written as*

$$R(g) = \begin{pmatrix} R^{(1)}(g) & 0 \\ 0 & R^{(2)}(g) \end{pmatrix}. \quad (20)$$

Then we have

$$C(R) = \{c_1 \mathbb{1}_{d_1} \oplus c_2 \mathbb{1}_{d_2} : c_1, c_2 \in \mathbb{C}\}. \quad (21)$$

Proof. Let T be a matrix with internal blocks $T_{1,1}, T_{1,2}, T_{2,1}, T_{2,2}$ given by

$$T = \begin{pmatrix} T_{1,1} & T_{1,2} \\ T_{2,1} & T_{2,2} \end{pmatrix}. \quad (22)$$

If $TX = XT$,

$$\begin{aligned} T_{1,1}R^{(1)} &= R^{(1)}T_{1,1}, & T_{1,2}R^{(2)} &= R^{(1)}T_{1,2}, \\ T_{2,1}R^{(1)} &= R^{(2)}T_{2,1}, & T_{2,2}R^{(2)} &= R^{(2)}T_{2,2}. \end{aligned}$$

Using Schur's lemma, we obtain $T_{1,1} = c_1 \mathbb{1}$, $T_{2,2} = c_2 \mathbb{1}$, $T_{1,2} = T_{2,1} = 0$. □

The situation is more complicated in cases where we have a direct sum of the same representation. In this case we find that the commutant is not simply a direct sum but allows for mixing between the irreps. As we see further below, this will correspond to mixing between elements of the repeated irreps which are the same.

Lemma 3. *We now consider a direct sum of the same representation $R = R^{(1)} \oplus R^{(1)}$. Then we have*

$$C(R) = \mathcal{M}_2(\mathbb{C}) \otimes \mathbb{1}_{d_1}. \quad (23)$$

Proof. As before, we write $T \in C(R)$ in a block-diagonal matrix. Then $TR = RT$ gives

$$T_{i,j}R^{(1)} = R^{(1)}T_{i,j}. \quad (24)$$

Schur's lemma implies that each $T_{i,j}$ is proportional to $\mathbb{1}$, i.e., $T_{i,j} = c_{i,j} \mathbb{1}$ for $c_{i,j} \in \mathbb{C}$. Thus we have

$$T = \begin{pmatrix} c_{1,1} \mathbb{1} & c_{1,2} \mathbb{1} \\ c_{2,1} \mathbb{1} & c_{2,2} \mathbb{1} \end{pmatrix} = \begin{pmatrix} c_{1,1} & c_{1,2} \\ c_{2,1} & c_{2,2} \end{pmatrix} \otimes \mathbb{1}. \quad (25)$$

□

Now let us generalise the above results. Let R be a representation of G on V . Then Maschke's theorem (for finite groups) or the Peter–Weyl Theorem (for Lie groups) asserts that V is decomposable into a direct sum of irreducible representations

$$V \simeq m_1 R^{(1)} \oplus m_2 R^{(2)} \oplus \cdots m_k R^{(k)}, \quad (26)$$

where $mR = R \oplus R \cdots \oplus R$ signifies m repetitions of the same representation, and $\{R^{(i)}\}$ are the different irreducible representations. Applying the above lemmas gives the following theorem.

Theorem 1. *Under the decomposition given by Eq. (26), the commutant is given by*

$$C(R) = \{\oplus_{i=1}^k (M_i \otimes \mathbb{1}_{d_i}) : M_i \in \mathcal{M}_{m_i}(\mathbb{C}) \text{ for all } i\} \quad (27)$$

where each d_i is the dimension of the representation $R^{(i)}$.

Given that a square matrix $M \oplus N$ is unitary iff M and N are both unitary matrices, we obtain the following corollary.

Corollary 1. *All unitary operators commuting with R are given by*

$$C(R) \cap \text{U}(d) = \{\oplus_{i=1}^k (U_i \otimes \mathbb{1}_{d_i}) : U_i \in \text{U}(m_i) \text{ for all } i\}, \quad (28)$$

where $d = \dim V = \sum_{i=1}^k m_i d_i$ is the dimension of V .

The Corollary tells us the exact form of intermediate unitary gates $P(\theta)$ we should use for $\text{SU}(2)$ equivariant gates, which is evident from the following example.

Example 1. *For a system with three qubits, we can decompose the space under $\text{SU}(2)$ as*

$$(\mathbb{C}^2)^{\otimes 3} \simeq J_{3/2} \oplus J_{1/2} \oplus J_{1/2}, \quad (29)$$

where J_s is a space of total spin s with dimension $2s + 1$. Note that the basis transformation from the computational basis to the total spin basis is nothing but the Schur transformation given in the previous section [Eq. 3]. We can now see that the unitary operators that commute with $\text{SU}(2)$ are given (up to a global phase) by

$$\left(\begin{array}{c|c} \mathbb{1}_4 & 0_4 \\ \hline 0_4 & U_2 \otimes \mathbb{1}_2 \end{array} \right), \quad (30)$$

which is the gate we defined in the previous section.

4.2 $\text{SU}(2)$ equivariant gates are generalised permutations

We now completely characterise $\text{SU}(2)$ equivariant gates for n qubits using the above results, by computing the multiplicity of each representation. Our main tool is the Schur–Weyl duality which posits the duality between the irreducible representation of the symmetric group S_n and that of $\text{SU}(2)$. Thus the multiplicity is given by the dimension of the corresponding irreducible representation of S_n .

Let us first define two group actions. For $U \in \text{SU}(2)$, we define its action on $(\mathbb{C}^2)^{\otimes n}$ as

$$U(|v_1\rangle \otimes |v_2\rangle \otimes \cdots \otimes |v_n\rangle) = |Uv_1\rangle \otimes |Uv_2\rangle \otimes \cdots \otimes |Uv_n\rangle, \quad (31)$$

where each v_i is a vector in \mathbb{C}^2 . In matrix form, this action is nothing but $U^{\otimes N}$.

Another group we consider is the symmetric group S_n . For $\alpha \in S_n$, we define

$$\alpha(|v_1\rangle \otimes |v_2\rangle \otimes \cdots \otimes |v_n\rangle) = |v_{\alpha^{-1}(1)}\rangle \otimes |v_{\alpha^{-1}(2)}\rangle \otimes \cdots \otimes |v_{\alpha^{-1}(n)}\rangle. \quad (32)$$

We can also write down a matrix representation of this group action. Let us consider a transposition $\tau = (a, b) \in S_n$ first, which just swaps the a -th and b -th qubit. In matrix form, this operation is written as

$$\tau = \frac{1}{2}\sigma^a \cdot \sigma^b + \frac{1}{2}\mathbb{1}, \quad (33)$$

where $\sigma^i = \{\sigma_x^i, \sigma_y^i, \sigma_z^i\}$ is a vector of Pauli matrices acting on the i -th qubit. As any permutation α in S_n can be decomposed into transpositions, i.e., $\alpha = \tau_k \cdots \tau_2 \tau_1$ where each $\tau_i = (a_i, b_i)$ is a transposition, we obtain

$$\alpha = \left(\frac{1}{2}\sigma^{a_k} \cdot \sigma^{b_k} + \frac{1}{2}\mathbb{1}\right) \cdots \left(\frac{1}{2}\sigma^{a_2} \cdot \sigma^{b_2} + \frac{1}{2}\mathbb{1}\right) \left(\frac{1}{2}\sigma^{a_1} \cdot \sigma^{b_1} + \frac{1}{2}\mathbb{1}\right). \quad (34)$$

A crucial property of those two group actions is that they commute with each other, i.e., $U\alpha = \alpha U$. One can easily check this for a product state

$$\begin{aligned} U\alpha(|v_1\rangle \otimes \cdots \otimes |v_n\rangle) &= U(|v_{\alpha^{-1}(1)}\rangle \otimes \cdots \otimes |v_{\alpha^{-1}(n)}\rangle) \\ &= |Uv_{\alpha^{-1}(1)}\rangle \otimes \cdots \otimes |Uv_{\alpha^{-1}(n)}\rangle \\ &= \alpha(|Uv_1\rangle \otimes \cdots \otimes |Uv_n\rangle) \\ &= \alpha U(|v_1\rangle \otimes \cdots \otimes |v_n\rangle), \end{aligned}$$

which can be extended linearly to all vectors in the space. Thus it follows that a permutation is an $SU(2)$ equivariant operation. This fact is also the basis of the Schur-Weyl duality which we introduce below.

Inspired by Ref. [26], we further consider an operator

$$Q = e^{\sum_{i=1}^k c_i \alpha_i} = \sum_{n=0}^{\infty} \frac{1}{n!} \left(\sum_{i=1}^k c_i \alpha_i\right)^n, \quad (35)$$

where $c_i \in \mathbb{C}$, which we call generalised permutations. From the expansion, we see that Q also commutes with $U \in SU(2)$, which implies that Q is an $SU(2)$ equivariant operation as well (albeit not unitary, in general). If we further restrict unitarity, i.e., an operator $e^{\sum_i c_i \alpha_i}$ with Hermitian $\sum_i c_i \alpha_i$, such an operator is an element of the set given by Eq. (28).

We now prove the converse of the above statement, which is the main result of this section: All $SU(2)$ equivariant unitary operators can also be written as a form of $\exp[\sum_{i=1}^k c_i \alpha_i]$. Even though this can be understood as a consequence of von Neumann's double commutation theorem (see e.g., Ref. [48]), here we provide a constructive proof with a concrete example. The first ingredient for the proof is the *Schur-Weyl duality*.

Theorem 2 (Schur-Weyl duality). *Under the group actions of $U \in SU(2)$ and the symmetric group $\alpha \in S_n$, the tensor-product space decomposes into a direct sum of tensor products of irreducible modules⁶*

⁶A vector space where the scalars are a ring.

that determine each other. Precisely, we can write

$$(\mathbb{C}^2)^{\otimes n} \simeq \bigoplus_D \pi_n^D \otimes J_D \quad (36)$$

where the summation is over the Young diagram D with n boxes and at most two rows. For each D with r_1 boxes in the first row and r_2 boxes in the second row, J_D is the irreducible representation of $SU(2)$ with total spin $J = (r_1 - r_2)/2$, and π_n^D is the irreducible representation of the symmetric group associated with the given Young diagram D .

We formally introduce the Young diagram and the irreducible representation of S_n in Appendix B. However, for the rest of discussion in this section, it is fine to skip the details and only consider the dimension of π_n^D , as we show in the following Corollary.

Corollary 2. *From the Schur-Weyl duality, one obtains*

$$(\mathbb{C}^2)^{\otimes n} \simeq \bigoplus_{i=0}^{\lfloor n/2 \rfloor} m_i J_{s_i} \quad (37)$$

where m_i is the dimension of the irreducible representation of S_n whose Young diagram D_i has $n - i$ boxes in the first row and i boxes in the second row, and $s_i = n/2 - i$ is the total spin.

The dimension of the irreducible representation can be computed using the Hook length formula. After some steps, one can obtain

$$m_i = \begin{cases} 1, & \text{if } i=0, \\ \binom{n}{i} - \binom{n}{i-1}, & \text{otherwise.} \end{cases} \quad (38)$$

We can now apply Corollary 1 to this decomposition to obtain all possible $SU(2)$ equivariant gates. Precisely, we obtain

$$U = \left\{ \bigoplus_{i=0}^{\lfloor n/2 \rfloor} (U_i \otimes \mathbb{1}_{d_i}) : U_i \in U(m_i) \right\} \quad (39)$$

In addition, as each $U(m_i)$ has m_i^2 independent generators, the total number of parameters is given by

$$\sum_{i=0}^{\lfloor n/2 \rfloor} m_i^2 = \frac{1}{n+1} \binom{2n}{n} \quad (40)$$

Note that Ref. [22] also presents the same result. We also note that, for a quantum gate, we can subtract one from this formula as there is a redundancy for the global phase.

Another ingredient we need is the completeness of the irreducible representation.

Theorem 3 (The density theorem [49]). *Let $V = \mathbb{C}^n$ be an irreducible finite dimensional representation of a group G , i.e., there is a map $R : G \rightarrow GL(\mathbb{C}^n)$. Then $\{R(g) : g \in G\}$ spans $\mathcal{M}_n(\mathbb{C})$.*

See, e.g., Ref. [50] for a proof. The theorem implies that for any $M \in \mathcal{M}_n(\mathbb{C})$, we can find $g_i \in G$ and $c_i \in \mathbb{C}$ such that $M = \sum_{i=1}^k c_i R(g_i)$ when $\mathbb{C}^{\otimes n}$ is the irreducible representation of G .

Using the Schur-Weyl duality and the density theorem, we now prove the equivalence between a generalised permutation group action and $SU(2)$ equivariant unitary gates.

Theorem 4. For any $SU(2)$ equivariant unitary gate T , we can find $c_i \in \mathbb{C}$ and $\alpha_i \in S_n$ such that

$$T = e^{\sum_{i=1}^k c_i \alpha_i}. \quad (41)$$

Proof. First, from Corollary 2, we obtain

$$(\mathbb{C}^2)^{\otimes n} \simeq \bigoplus_{i=0}^{\lfloor N/2 \rfloor} m_i J_{s_i}. \quad (42)$$

Then let H be the generator of T , i.e., $T = e^{iH}$ and H is a Hermitian matrix. Looking at Corollary 1, we can move from the description of equivariant unitaries to their generators and see that H can be written as

$$H = \bigoplus_i h_i \otimes \mathbb{1}_{2s_i+1} = \sum_i h_i P_i \quad (43)$$

where h_i is a hermitian matrix in $\mathcal{M}_{m_i}(\mathbb{C})$ and P_i is a projector onto a subspace with total spin $2s_i + 1$. From the density theorem, one can find $\{c_{ij} \in \mathbb{R}\}$ and $\{\alpha_{ij} \in S_n\}$ such that $h_i = \sum_j c_{ij} \alpha_{ij}$ for each i . Moreover each projector P_i can be written as

$$P_i = \prod_{j \neq i} \frac{J^2 - s_j(s_j + 1)}{s_i(s_i + 1) - s_j(s_j + 1)}, \quad (44)$$

where $\mathbf{J} = \sum_{i=1}^n \boldsymbol{\sigma}^i / 2$ is the total spin operator and $J^2 = \mathbf{J} \cdot \mathbf{J}$. As J^2 has eigenvalues $s_i(s_i + 1)$ for each subspace J_{s_i} , one can verify that the given operator is indeed a projector. After rewriting

$$J^2 = \frac{1}{4} (3n + \sum_{i \neq j} \boldsymbol{\sigma}^i \cdot \boldsymbol{\sigma}^j) = \frac{4n - n^2}{4} + \sum_{i > j} (i, j) \quad (45)$$

where (i, j) is a transposition, we see that $J^2 \in \mathbb{R}[S_n]$. If we again look at Eq. (43), we can now see that as $h_i, P_i \in \mathbb{R}[S_n]$ our unitary $T = e^{iH}$ is indeed an exponentiated sum of permutations with coefficients in \mathbb{C} . \square

4.3 Twirling and permutations

In Ref. [24], the Twirling method is proposed to construct an equivariant unitary gate. For a given Hermitian matrix H which is the generator of a unitary gate $V = \exp(iH)$ and a Lie group \mathcal{G} , one obtains an equivariant version of it using the twirling formula:

$$\mathcal{T}_U[H] = \int d\mu(g) R(g) H R(g)^\dagger, \quad (46)$$

where $\mu(g)$ is the Haar measure for the Lie group \mathcal{G} . Then $\mathcal{T}_U[H]$ commutes with any $h \in \mathcal{G}$ due to a defining property of the Haar measure, and so does the gate $\exp\{i\mathcal{T}_U[H]\}$.

We now show that for $\mathcal{G} = \text{SU}(2)$, the twirling formula yields a generalised permutation. For a Hermitian matrix $H \in \mathcal{M}_{2^n}(\mathbb{C})$, we obtain

$$\begin{aligned}\mathcal{T}_U[H] &= \int d\mu(g) R(g) H R(g)^\dagger \\ &= \int_U dU U^{\otimes n} H (U^\dagger)^{\otimes n} \\ &= \sum_{\sigma, \tau \in S_n} \mathcal{W}g(\sigma^{-1}\tau, d) \text{Tr}[H\tau]\sigma,\end{aligned}\tag{47}$$

where $d = 2^n$ is the dimension of the Hilbert space, $\mathcal{W}g(\sigma, d)$ is the Weingarten function, and we identified $\sigma, \tau \in S_n$ as an operator using the representation (see e.g., Refs. [48, 51] for the explanation how the last line is obtained). Ultimately this is a permutation scaled by a real coefficient as required. Furthermore, as $\mathcal{T}_U[H]$ is also Hermitian by definition, we know that $\mathcal{T}_U[H]$ is a Hermitian element of $\mathbb{C}[S_n]$, which can be a generator for an equivariant unitary gate.

On the other hand, all generators of equivariant gates can be obtained from the twirling formula. In the spin-basis, we know that each generator of an equivariant gate is given by Eq. (43), i.e., $H \simeq \oplus_i h_i \otimes I_{d_i}$ (where the dimension of h_i and d_i are obtained from the Schur-Weyl duality). As this is an element of the commutant [Eq. (27)], H is also equivariant, i.e., $HU^{\otimes N} = U^{\otimes N}H$, so $\mathcal{T}_U[H] = H$. In other words, the set of all generators of equivariant gates and the set of all twirled generators are the same:

$$\begin{aligned}\{H \in \mathcal{M}_{2^n}(\mathbb{C}) : U^{\otimes n} e^{iH} &= e^{iH} U^{\otimes n} \text{ for all } U \in \text{SU}(2) \text{ and } H = H^\dagger\} \\ &= \{\mathcal{T}_U[H] : H \in \mathcal{M}_{2^n}(\mathbb{C}) \text{ and } H^\dagger = H\}.\end{aligned}\tag{48}$$

4.4 Revisiting three-qubit $\text{SU}(2)$ equivariant gates

In this subsection, using the three-qubit vertex gate as an example, we illustrate how to represent our equivariant gates as elements of $\mathbb{C}[S_n]$. We apply Theorem 4 to the three-qubit gate we have found in Sec. 3, using the Schur map given in Eq. (16). A direct consequence of the Schur transform is that it defines invariant subspaces under $U^{\otimes 3}$ for any $U \in \text{SU}(2)$, given by $J_{3/2} = \text{span}\{S_3^\dagger |0\rangle, S_3^\dagger |1\rangle, S_3^\dagger |2\rangle, S_3^\dagger |3\rangle\}$, $J_{1/2}^a = \text{span}\{S_3^\dagger |4\rangle, S_3^\dagger |5\rangle\}$, and $J_{1/2}^b = \text{span}\{S_3^\dagger |6\rangle, S_3^\dagger |7\rangle\}$. From the structure of $P(\vec{\theta})$, we know the gate has four generators given by $\{G_I := \mathbf{0}_4 \oplus \mathbb{1}_4, G_X := \mathbf{0}_4 \oplus (X \otimes \mathbb{1}_2), G_Y := \mathbf{0}_4 \oplus (Y \otimes \mathbb{1}_2), G_Z := \mathbf{0}_4 \oplus (Z \otimes \mathbb{1}_2)\}$, where $\mathbf{0}_4$ acts on $J_{3/2}$ whereas X, Y, Z mixes $J_{1/2}^a$ and $J_{1/2}^b$. One can also see that a permutation in S_3 mixes subspaces $J_{1/2}^a$ and $J_{1/2}^b$ (whereas it acts trivially on $J_{3/2}$ subspace).

A matrix representation of a permutation for $\{J_{1/2}^a, J_{1/2}^b\}$ is obtained by applying each permutation

to a basis vector, which is given as

$$(1, 2) = \begin{pmatrix} 1 & 0 \\ 0 & -1 \end{pmatrix} \otimes \mathbb{1}_2 = Z \otimes \mathbb{1}_2 \quad (49)$$

$$(2, 3) = \begin{pmatrix} -1/2 & -\sqrt{3}/2 \\ -\sqrt{3}/2 & 1/2 \end{pmatrix} \otimes \mathbb{1}_2 = -\frac{1}{2}Z \otimes \mathbb{1}_2 - \frac{\sqrt{3}}{2}X \otimes \mathbb{1}_2 \quad (50)$$

$$(1, 3) = \begin{pmatrix} -1/2 & \sqrt{3}/2 \\ \sqrt{3}/2 & 1/2 \end{pmatrix} \otimes \mathbb{1}_2 = -\frac{1}{2}Z \otimes \mathbb{1}_2 + \frac{\sqrt{3}}{2}X \otimes \mathbb{1}_2, \quad (51)$$

Each matrix should be read as follows. For example, if we apply $(2, 3)$ to $S_3^\dagger |4\rangle$, we have

$$(2, 3)S_3^\dagger |4\rangle = -\frac{1}{2}S_3^\dagger |4\rangle - \frac{\sqrt{3}}{2}S_3^\dagger |6\rangle, \quad (52)$$

where the coefficients are from the first column of the matrix representation of $(2, 3)$. Note that the permutation transforms $S_3^\dagger |5\rangle$ exactly the same way (but mixes $S_3^\dagger |5\rangle$ and $S_3^\dagger |7\rangle$). Using the above expressions, remaining elements are obtained as follows (where we dropped $\otimes \mathbb{1}_2$ to simplify the notation):

$$(1, 2, 3) = (1, 2)(2, 3) = -\frac{1}{2}\mathbb{1} - i\frac{\sqrt{3}}{2}Y \quad (53)$$

$$(1, 3, 2) = (1, 2)(1, 3) = -\frac{1}{2}\mathbb{1} + i\frac{\sqrt{3}}{2}Y. \quad (54)$$

Thus we have

$$I = 1, \quad X = -\frac{2}{\sqrt{3}}[(2, 3) + 1/2(1, 2)] \quad (55)$$

$$Y = i\frac{1}{\sqrt{3}}[2(1, 2, 3) + 1], \quad Z = (1, 2). \quad (56)$$

However, these operators cannot be generators of our gate as they do not annihilate the $J = 3/2$ subspace (recall that our generators have $\mathbf{0}_4$ on the $J_{3/2}$ subspace). Thus we need a projector to the $J = 1/2$ subspace, which is given by

$$P_{J=1/2} = \frac{J^2 - 15/4}{3/4 - 15/4} = \frac{5}{4} - \frac{1}{3}J^2 \quad (57)$$

where J^2 is

$$J^2 = \frac{1}{4}[\boldsymbol{\sigma}_1 + \boldsymbol{\sigma}_2 + \boldsymbol{\sigma}_3]^2 = \frac{3}{4} + [(1, 2) + (2, 3) + (1, 3)]. \quad (58)$$

By combining the projector and expressions of Pauli operators in $J = 1/2$ subspaces, we can write

three generators as

$$G_I = 1 - \frac{1}{3}[(1, 2) + (2, 3) + (1, 3)] \quad (59)$$

$$G_X = -\frac{2}{\sqrt{3}}\left[-\frac{1}{2} + (2, 3) + \frac{1}{2}(1, 2) - \frac{1}{2}(1, 2, 3) - \frac{1}{2}(1, 3, 2)\right] \quad (60)$$

$$G_Y = i\frac{1}{\sqrt{3}}\left[1 + 2(1, 2, 3) - (1, 2) - (2, 3) - (1, 3)\right] \quad (61)$$

$$G_Z = (1, 2) - \frac{1}{3}[1 + (1, 3, 2) + (1, 2, 3)] \quad (62)$$

One can check that each generator annihilates the $J_{3/2}$ subspace (e.g., $G_X |000\rangle = 0$), and acts like a Pauli gate between the $J_{1/2}^a$ and $J_{1/2}^b$ subspaces (e.g., $G_X S_3^\dagger |5\rangle = S_3^\dagger |7\rangle$). Also note that, as there is a freedom in choosing two $J = 1/2$ subspaces (any unitary mixtures between $J_{1/2}^a$, $J_{1/2}^b$ are also valid subspaces), the exact form of generators $\{G_I, G_X, G_Y, G_Z\}$ depends on the specific choice of the Schur gate S_3 (which is from Eq. (16) for our case).

To summarise, any SU(2) equivariant gate on the three qubit can be written as

$$V(\vec{\theta}) = S_3^\dagger P(\vec{\theta}) S_3 = \exp\left[i\{\theta_0 G_I + \theta_1 G_X + \theta_2 G_Y + \theta_3 G_Z\}\right], \quad (63)$$

which is a generalised permutation from Eq. (59-62).

We now answer the question raised at the end of the previous section. If we apply our three-qubit gate to 3rd, 4th, and 7th qubits among 8 qubits, we first obtain its representation as a generalised permutation between those qubits, and apply it to basis vectors of a global spin subspaces. For example, G_X for those qubits are given as

$$G_X^{(3,4,7)} = -\frac{2}{\sqrt{3}}\left[-\frac{1}{2} + (4, 7) + \frac{1}{2}(3, 4) - \frac{1}{2}(3, 4, 7) - \frac{1}{2}(3, 7, 4)\right]. \quad (64)$$

Then one can construct its matrix form in a certain subspace (e.g. one of the J_2 subspaces) by applying it to the basis vectors of the subspace. Then the gate $\exp[-i\theta G_X^{(3,4,7)}]$ can be reconstructed by applying the exponential map.

We finalise this section by introducing an alternative description of these generators using the scalar products. For three operator vectors $\sigma_1, \sigma_2, \sigma_3$, the only possible scalar operators (that are invariant under the group transformation) obtained from those operators are $\sigma_1 \cdot \sigma_2, \sigma_2 \cdot \sigma_3, \sigma_1 \cdot \sigma_3$, and $\sigma_1 \cdot (\sigma_2 \times \sigma_3)$ up to constant factors, where $A \times B$ is the cross product between two vectors. Thus another possible representation of a parameterised three-qubit equivariant gate is

$$W = \exp\left[i(\theta_{12}\sigma_1 \cdot \sigma_2 + \theta_{23}\sigma_2 \cdot \sigma_3 + \theta_{13}\sigma_1 \cdot \sigma_3) + i\phi\sigma_1 \cdot (\sigma_2 \times \sigma_3)\right]. \quad (65)$$

Then it can be shown that this gate is the same as $V(\vec{\theta})$ up to a global phase.

Using

$$\begin{aligned} (\sigma_1 \cdot \sigma_2)(\sigma_2 \cdot \sigma_3) &= \sum_{a \in \{x, y, z\}} \sum_{c \in \{x, y, z\}} \sigma_1^a \sigma_2^a \sigma_2^c \sigma_3^c \\ &= \sum_{a \in \{x, y, z\}} \sum_{c \in \{x, y, z\}} \delta_{ac} \sigma_1^a \sigma_3^c + i \sum_{b \in \{x, y, z\}} \epsilon_{abc} \sigma_1^a \sigma_2^b \sigma_3^c \\ &= \sigma_1 \cdot \sigma_3 + i\sigma_1 \cdot (\sigma_2 \times \sigma_3), \end{aligned} \quad (66)$$

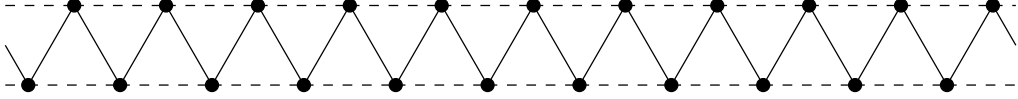


Figure 6: A one dimensional triangular lattice. We solve the Heisenberg model defined on this lattice using the equivariant gates. The interaction strength between qubits linked with solid lines is given by J_1 whereas those between qubits linked with dash lines are J_2 .

and Eq. (33), we obtain

$$2i\sigma_1 \cdot (\sigma_2 \times \sigma_3) = [\sigma_1 \cdot \sigma_2, \sigma_2 \cdot \sigma_3] = [2(1, 2) - 1, 2(2, 3) - 1] = 4(1, 2, 3) - 4(1, 3, 2). \quad (67)$$

In addition, we need another identity $P_{J=3/2}^2 = P_{J=3/2}$, which gives

$$(1, 2, 3) + (1, 3, 2) = (1, 2) + (2, 3) + (1, 3) - 1. \quad (68)$$

Note that this equality only implies that the LHS and RHS act the same on our vector space. Of course, they are different elements in $\mathbb{C}[S_n]$.

Combining all these together, we can write each generator of W in terms of $\{G_I, G_X, G_Y, G_Z\}$ as

$$\sigma_1 \cdot \sigma_2 = 2(1, 2) - 1 = 1 - 2G_I + 2G_Z \quad (69)$$

$$\sigma_2 \cdot \sigma_3 = 2(2, 3) - 1 = 1 - 2G_I - \sqrt{3}G_X - G_Z \quad (70)$$

$$\sigma_3 \cdot \sigma_1 = 2(1, 3) - 1 = 1 - 2G_I + \sqrt{3}G_X - G_Z \quad (71)$$

$$\sigma_1 \cdot (\sigma_2 \times \sigma_3) = -\frac{i}{2}[4(1, 2, 3) - 4(1, 3, 2)] = -2\sqrt{3}G_Y, \quad (72)$$

which implies that W is just another parameterisation of $V(\vec{\theta})$ (up to a global phase).

5 Numerical Simulations

In this section, we numerically demonstrate the efficacy of our equivariant gates for solving quantum many-body Hamiltonians. Our Hamiltonians are Heisenberg models (which are rotationally invariant) defined on frustrated lattices. Even though the Heisenberg models are toy models, they play an important role in understanding low-temperature physics of some exotic materials [52]. All numerical simulations in this section were performed using the PennyLane [53] software package with the Lightning [54] plugin. Relevant source code is available in GitHub repository [55].

5.1 One dimensional triangular lattice

Let us first consider a one-dimensional triangular lattice given as in Fig. 6. The Hamiltonian we want to solve is

$$H = J_1 \sum_{i=1}^n [\sigma_i^x \sigma_{i+1}^x + \sigma_i^y \sigma_{i+1}^y + \sigma_i^z \sigma_{i+1}^z] + J_2 \sum_{i=1}^n [\sigma_i^x \sigma_{i+2}^x + \sigma_i^y \sigma_{i+2}^y + \sigma_i^z \sigma_{i+2}^z], \quad (73)$$

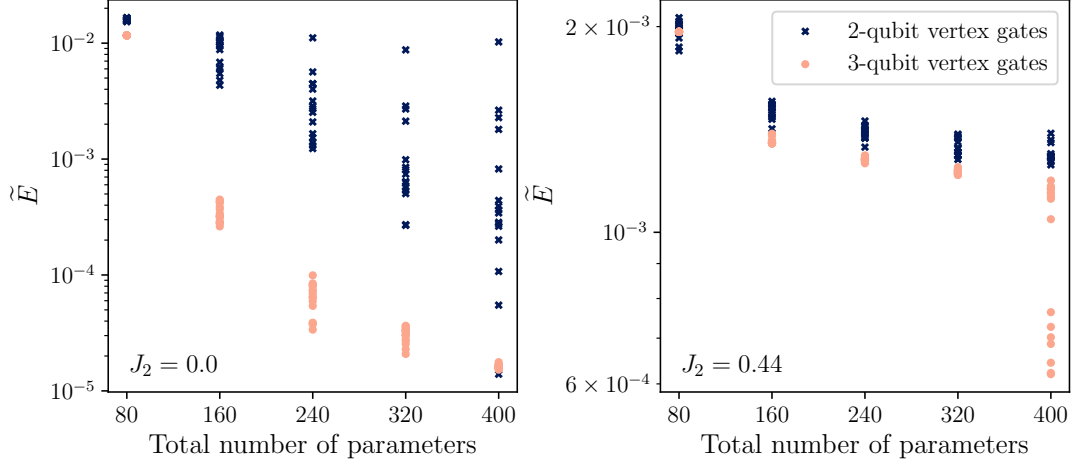


Figure 7: Normalised converged energies as functions of the total number of parameters in a given ansatz for $J_2 = 0.0$ (left) and $J_2 = 0.44$ (right). Each datapoint represents the converged energy obtained from an initial parameter.

where we impose the periodic boundary condition $\sigma_{n+1}^{x,y,z} = \sigma_1^{x,y,z}$. Throughout the section, we fix $J_1 = 1$ and consider $J_2 \in \{0, 0.44\}$. When $J_2 = 0$, the Hamiltonian can be transformed into a stoquastic form [56] and a classical algorithm, the variational quantum Monte Carlo (vQMC) with a simple complex-valued restricted Boltzmann machine (RBM), can find the ground state energy extremely accurately [57]. In contrast, such a transformation does not work for $J_2 \gtrsim 0$ [29] and the vQMC with the RBM deviates from the true ground state. We here choose $J_2 = 0.44$ as a recent study [58] reported that such a deviation is maximised near this value. Still, we note that the density matrix renormalization group can faithfully solve our model as the model is one-dimensional.

We compare the performance of two ansätze for solving this Hamiltonian. The first ansatz only uses the two-qubit vertex gates, which is given by

$$|\psi(\{\theta\})\rangle = \prod_{i=p}^1 \left[\prod_{j=1}^n V_{j,j+2}(\theta_{i,j+n}) \prod_{j=1}^{n/2} V_{2j,2j+1}(\theta_{i,j+n/2}) \prod_{j=1}^{n/2} V_{2j-1,2j}(\theta_{i,j}) \right] |\psi_0\rangle, \quad (74)$$

where V_{kl} is the two-qubit vertex gate acting on k -th and l -th qubits and $|\psi_0\rangle = (|01\rangle - |10\rangle)^{\otimes n/2} / \sqrt{2}^{n/2}$ is a series of singlets. As $|\psi_0\rangle$ is $SU(2)$ invariant and our circuit is $SU(2)$ equivariant, the output state is also $SU(2)$ invariant. The ansatz has a total of $2np$ parameters where p is the number of blocks in the ansatz.

Likewise, we also define the second ansatz which consists of the three-qubit vertex gates as

$$|\psi(\{\theta_{i,j}\})\rangle = \prod_{i=p}^1 \left[\prod_{j=1}^n V_{j,j+1,j+2}(\{\theta_{i,4j-3}, \theta_{i,4j-2}, \theta_{i,4j-1}, \theta_{i,4j}\}) \right] |\psi_0\rangle, \quad (75)$$

where $V_{j,j+1,j+2}$ is the three-qubit vertex gate acting on qubits $\{j, j+1, j+2\}$. Also recall that the

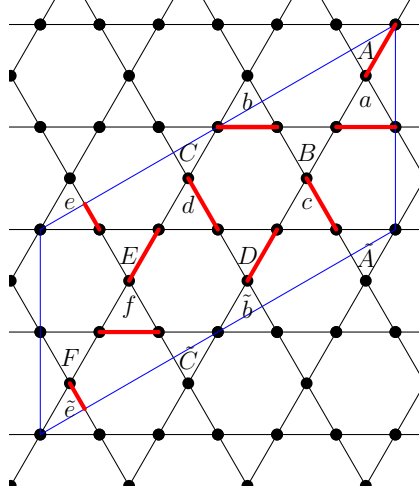


Figure 8: The Kagome lattice. We choose a unit cell with $N = 18$ spins enclosed by blue lines. Red links indicate the singlets which we use as an initial state. Our variational circuit is constructed by applying three-qubit vertex gates to each triangle (a - f and A - F). See the main text for details.

three-qubit vertex gate has four parameters, so the ansatz has in total $4np$ parameters.

We now solve the Hamiltonian from Eq. (73) with $n = 20$ for two different values of $J_2 \in \{0.0, 0.44\}$ using the two proposed ansätze by simulating variational quantum eigensolvers (VQEs) using a classical simulator. For each ansatz, we optimise the parameters by minimizing $\langle H \rangle$ using the Adam optimiser. We then compute the converged normalised energies $\tilde{E} = (\langle H \rangle - E_{\text{GS}})/|E_{\text{GS}}|$ where E_{GS} is the true ground state energy obtained from exact diagonalization. For the ansatz with two-qubit vertex gates, we use the number of blocks $p = [2, 4, 6, 8, 10]$. On the other hand, $p = [1, 2, 3, 4, 5]$ are used for the ansatz with three-qubit vertex gates. In addition, inspired by Ref. [59], we initialise the parameters using samples from the distribution $\mathcal{U}_{[0, \alpha]}/(\text{total number of parameters})$ where $\mathcal{U}_{[0, \alpha]}$ is the uniform distribution between 0 and α , and α is a hyperparameter giving a relative scaling. We also note that our simulation is performed by computing exact gradients (without shot noise), which is more efficient for classical simulators.

For 16 random initial parameters, we plot the converged normalised energies in Fig. 7 as a function of the total number of parameters. We observe that the converged normalised energies from the ansatz with three-qubit vertex gates are generally closer to the true ground state energy. Especially, when $J_2 = 0.44$, the converged energy from the three-qubit vertex gates decreases as the number of parameter increases, whereas that from the two-qubit vertex gates gets flat. This example shows that using a multi-qubit vertex gate is helpful even for solving a Hamiltonian with two-body interactions. We expect that this is because the circuit ansatz with three-qubit vertex gates is more expressive than that of two-qubit vertex gates when the same number of parameters is provided.

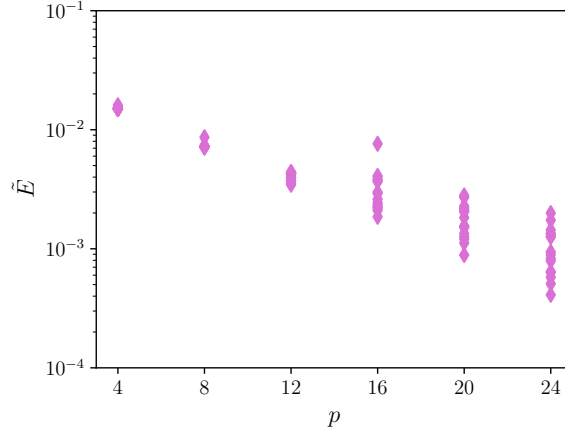


Figure 9: Converged normalised energies as a function of circuit depths for the Heisenberg model on the Kagome lattice. For each value of p , 18 random initial parameters are sampled. For each random initial parameter, full VQE simulation is performed and the converged energy is shown.

5.2 Kagome lattice

We now extend the previous result to study the model on the Kagome lattice. We consider an $n = 18$ unit cell from the lattice with periodic boundary condition. Our choice of the unit cell is depicted in Fig. 8.

Formally, the Hamiltonian of the system is written as

$$H = \sum_{\langle i,j \rangle} [X_i X_j + Y_i Y_j + Z_i Z_j] \quad (76)$$

where the summation is over all nearest neighbours in the lattice.

We construct an ansatz using three-qubit vertex gates as

$$|\psi(\{\theta_{i,j}\})\rangle = \prod_{i=p}^1 \prod_{j=A}^F V_j(\theta_{i,j}) \prod_{j=a}^f V_j(\theta_{i,j}) |\psi_0\rangle \quad (77)$$

where $V_{a,\dots,f}$ ($V_{A,\dots,F}$) are the three-qubit vertex gates acting on vertices of each triangle a to f (A to F , respectively; see Fig. 8). As each block has 12 gates, the total number of parameters is $48p$ (recall that each three-qubit vertex gate has four parameters). We also use a series of singlets as an initial state, where each singlet is indicated by a red link in Fig. 8. Formally, we can write

$$|\psi_0\rangle = \frac{1}{\sqrt{2}^{n/2}} \bigotimes_{\{i,j\} \in S} (|01\rangle - |10\rangle)_{ij}$$

where S is the set of all links.

We numerically optimise the parameters of the circuit by minimizing $\langle H \rangle$. The Adam optimiser is used with the same parameter initialization techniques as in the previous example. We plot the converged

normalised energies as a function of p in Fig. 9. The plot shows that the best converged energies decrease nearly exponentially with p . The smallest converged normalised energy is $\tilde{E} \approx 5.7 \times 10^{-4}$ obtained from $p = 24$, which is comparable to data obtained in Refs. [60, 61] using different ansätze.

To summarise, we have shown that the three-qubit vertex gate introduced in the previous sections is useful for solving the Heisenberg model on different lattices. Given the efficacy of our equivariant gates for solving the ground state problem, we also expect that one can construct a QML model using our gates to classify rotationally invariant datasets such as point clouds [62]. However, as a QML model for those datasets without classical pre-processing requires a large number of qubits beyond the reach of a classical simulator (which is about $\lesssim 30$ qubits), we leave it for future study.

6 Connections and discussions

Throughout the previous sections, we have introduced an elegant construction method for $SU(2)$ equivariant quantum circuits based on the Schur transformation. Those circuits can be naturally seen as a spin network which is a tensor network of group-invariant tensors. We have further developed a theory of the $SU(2)$ equivariant gates from the Schur-Weyl duality, relating our gates to other known constructions based on the twirling formula and generalised permutations.

As spin networks and quantum circuits for permutations appear in lots of different contexts in the field of high energy physics and theoretical quantum computations, we discuss various connections to other fields of research as well as possible future directions of study in the following.

6.1 PQC, PQC+, and non-classical heuristic algorithms

The idea of taking spins and coupling them is reminiscent of a computational model already seen in the literature. This idea is at the heart of what we mentioned above is called permutational quantum computing (PQC) which is centered around the computational class PQC and the closely related PQC+[31, 20]. This class of problems is important as they provide strong evidence that the transition from permutations to exponentiated sums of the generators of permutations marks a transition to classically hard sampling tasks.

The PQC model In short, PQC is a model of quantum computing that is intimately tied to the structure of a *binary tree* coupling of spins. The original idea stemmed from the notion that spin networks could form a model of quantum computing [43]. In an attempt to extract a formal computational class from this model, PQC was introduced which only considers tree-like structures [31]. To achieve this, we take n -spins and choose a particular ordering to add the qubits to the already coupled spins (which we can see as a choice of what sequence of spins to apply the J^2 operator to). The possible outcomes of this chosen order of spin recoupling along with the addition of the possible total angular momentum outcomes gives an alternative basis.

PQC is the computational class of problems described as a permutation circuit set between two coupled spin-basis states. Given a permutation operator U_σ representing the unitary composed of swap

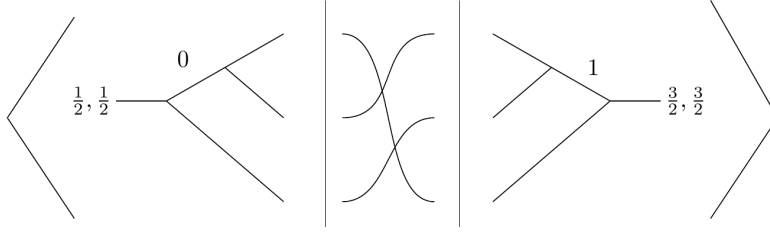


Figure 10: A PQC calculation is an expectation value of a permutation of qubits in the spin-coupling basis.

gates implementing the permutation $\sigma \in S_n$, PQC is the set of problems written as:

$$\langle v' | U_\sigma | v \rangle = \langle b' | S^\dagger U_\sigma S | b \rangle \quad (78)$$

where b is some binary label for the computational basis and S is the schur gate. The reason Schur gate is a core component in PQC is because PQC states are simply elements of the spin basis.

The Schur gate is the preparation procedure that sends qubit basis states to spin states. In the PQC literature, these states are often presented by PQC coupling diagrams of the kind seen in Fig. 2. Practically a standard PQC calculation is merely the inner-product between two Schur gates applied to some computational basis states with some SWAP gates in between them. It was shown that this model is in fact classically simulable in large part due to the particular tree like structure of binary spin-recoupling and the restrictions this tacitly forces on the Clebsch-Gordan coefficients dictating their coupling [32]. An immediate observation we can make, given our above discussion on spin networks, is that PQC diagrams, which we take to be sequentially coupled spin-1/2s, are spin networks with their external wires fixed to specific J_z values. Each PQC basis element is a member of the collection of spin networks of the same tree structure permissible by the recoupling of their spins and a J_z value angular state at the end of the tree.

PQC+ Despite the initial disappointment that PQC was in fact classically simulable, it has been generalised to a broader model that is believed to be unlikely to have this property. The extended model is known as PQC+ where instead of working with a permutation $\sigma \in S_n$, we work with unitaries generated by sums of elements of the permutation algebra $\mathbb{C}[S_n]$: this is composed of elements $f = \sum_i c_i \sigma_i$ with $U_f = e^{if} = e^{i \sum_k c_k \sigma_k}$ so in the end computations are defined in the following manner:

$$\langle v' | U_f | v \rangle. \quad (79)$$

As was mentioned above, the belief in the resilience of this model to ‘dequantisation’⁷ rests on the fact that PQC+ is capable approximately computing unitary S_n Fourier coefficients in polynomial time, the details can be found in Ref. [26]. The general idea is that, much like in a traditional Fourier transform, to calculate the Fourier coefficient of any element one must get the component from every element in the original basis, so in the worst case classically one must go through as many components as there are basis elements. For an S_n Fourier transform there are a permutational number of elements⁸, as

⁷Quantum computing short hand for the situation where a quantum algorithm is proposed to be faster than possible classical alternatives only for a new classical method to be devised that eliminates this speed-up.

⁸This is sloppy, as one actually runs over the number of irreps which slightly smaller than permutationally, i.e., factorially, large but remains super-exponential.

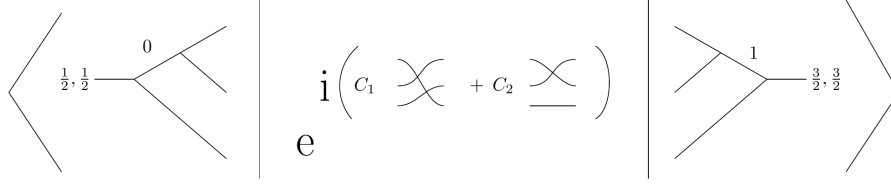


Figure 11: A PQC+ calculation is the exponent of a linear combination of the generators of permutations. We note that, previously in Fig. 10, the permuted wires stand for the actual permutation, while here they stand for the generators.

such even an approximate classical polynomial time algorithm to compute the worst case is unlikely. It is this property that relates to claims of super-exponential speed-up as permutational complexity grows considerably faster than the exponential. For more details we direct the reader to Refs. [26, 20] where one also finds some practical application of this in condensed matter calculations in accessing coefficients relevant for the Heisenberg chain.

Spin-network circuits as *non-classical heuristics* The major observation in the work on PQC+ is that, for a Hamiltonian written $H = \sum_i c_i \sigma_i$, we can approximate $\langle u | \exp(-itH) | v \rangle$ in polynomial time using a quantum circuit. As the Hamiltonian is in the space $\mathbb{C}[S_n]$ (the algebra of permutations), we are computing $\mathbb{C}[S_n]$ Fourier coefficients in polynomial time. This computation of a Fourier coefficient using the best-known classical algorithm requires one to run over all of S_n which is super-exponential in size thus this suggests a super-exponential speed-up. This suggests that in general elements of the form $\langle u | e^{i \sum_k c_k \sigma_k} | v \rangle$ cannot be efficiently classically computed [20]. These elements however are exactly the form of our parameterised vertex gates – this tells us that the paths through parameter space our vertex gates move through are in general classically inaccessible. This motivates us to introduce the term *Non-classical heuristics* – parameterised ansätze that are defined as moving through spaces that cannot be accessed classically in polynomial time. We should note however that this idea does not tell us if moving through this space is a useful thing to do; the space may still be barren. We have shown that the form of these problems matches those of $SU(2)$ (perhaps more generally $SU(d)$) equivariant gates which are of direct practical interest. The principle then is that there could be practical problems, such as $SU(2)$ equivariant optimisation problems, for which we can design quantum circuit heuristics, such as spin-network circuits, that cannot be replicated classically because of the maps they implement cannot be replicated in polynomial time.

In terms of the approaches to machine learning presented in PQC+ to-date and our spin-network circuits, it should be noted that there is a technical distinction between the methods used. The PQC+ focuses on tuning the coefficients c_i of the exponent $\sum_i c_i \sigma_i \in \mathbb{C}[S_n]$. In our spin-network circuits we parameterise the $SU(2)$ distinguishable spin-spaces and mix spin irreps of the same J -value in the Schur-Weyl decomposition via unitaries (see Corollary 1). Though both exist in the same space the way in which one moves through that parameter space is very different.

6.2 Further directions

Mixed valency networks In this work, we have focused on the traditional spin network perspective where the same valency exists throughout the graph. In the usual contexts for spin networks, there is a

physical motivation for this (see Appendix C). However, from a quantum algorithms perspective, there is no fundamental reason not to mix the valencies. While it is true that larger vertex maps are likely more expressive than small ones as they are generated by a larger set of permutations, it could also be possible that an architecture with small vertex ones are advantageous for practical training.

***G*-Networks** The idea of graphs with edges indexed by representations of a group in the manner presented here is more general than $SU(2)$. The most obvious extension is to $SU(N)$ for which many of the technical elements used in the $SU(2)$ still remain. In particular, we have generalised Clebsch-Gordan coefficients. Thus we can still decompose products of irreps into block diagonal form allowing us to express the idea of coupling two representations and presenting this as a collection of irrep indexed diagrams. These can then be parameterised in the manner used throughout this paper to create general parameterised equivariant maps suitable for machine learning. In the specific case of $SU(N)$, there is reason to believe that the same hopes of finding algorithms particularly suited to quantum computing remains: Namely because the speed-up arguments presented in Ref. [20] apply to $SU(N)$. From an applications perspective this would allow for this research to connect to condensed matter physics which would be an excellent candidate domain for such non-classical heuristic algorithms [63, 64, 65]. Leaving $SU(2)$ for higher dimensions, however, is not without complications. One striking difference is that while with $SU(2)$ we have one irreducible representation per dimension, the size of which identifies the representation, for $SU(N)$ the irreps are identified by ‘highest weights’ which are $N - 1$ (half) integers that provide representations only in certain dimensions. While this may be surmountable, it is likely that general G -networks will be markedly more complex than spin networks.

Implicitly, we are relying on the ability to construct all representations from irreducible ones, which tells us that our groups of interest will typically also need a notion of compactness, or that the situation of interest is restricted to elements where irreducible deconstruction can be relied upon. Without this guarantee, we cannot expect that it is enough to identify a structure of irreducible representations to construct the other representations. An interesting perspective on this direction is that it can be seen as fusing the perspective of equivariant QML algorithms with work done in tensor networks. Indeed a spin network is essentially a tensor network decomposition of some map where the tensors involved are always $SU(2)$ invariant. The general version of this through G -networks is essentially tensor network decomposition of G -equivariant maps into G -invariant ‘harmonic’ tensors.

Quantum Gravity While the connection to the field of Loop Quantum Gravity (LQG) has only been indirectly alluded to in this work, it holds a natural significance. In LQG, space itself is a quantum state on which geometric operators act to give values for length, area, angle, and volume. The basis of its state space is made up of spin networks. A more detailed explanation of this can be found in Appendix C.

As with all theories of quantum gravity, LQG faces a general lack of decisive experimental data. However, our research demonstrates that quantum computing has the potential to represent some of the fundamental mathematical structures that underlie the quantised nature of space in LQG. This opens up the possibility for exploring these structures numerically using quantum computing devices.

While in LQG, the dynamics of spin networks often involve broader groups such as $SL(2; \mathbb{C})$ that correspond to relativistic symmetries, we still find value in the $SU(2)$ (Euclidean) models. This is because even in the most developed LQG models addressing quantised relativistic space-time, the states of space themselves are still projected onto $SU(2)$ [66]. In summary, though tackling the full dynamics

directly might prove challenging through this approach, exploring the kinematic aspects is well within reach. Interestingly, the PQC literature already contains the treatment of a limited class of spin networks to calculate the Ponzano-Regge amplitudes [31] which are the transition amplitudes for the topological quantum field theory known as the Ponzano-Regge model which itself is studied as a model for quantum gravity [67]. In this context, spin networks are not viewed as states, but rather as transition maps in a 2+1 euclidean gravity setup, i.e., non-relativistic dynamics over lower dimensions (see Appendix C for details). While there might be an absence of the full group of relativistic symmetries, investigating even a simplification of these transition amplitudes and the associated objects, termed spinfoams, could yield valuable insights.

An additional observation, mentioned above in a different context, is the possibility of generalising the models we have explored. This includes considering networks with mixed vertices or looking into groups like $SU(N)$, which extend beyond what is typically seen in LQG. Indeed in LQG, even models with vertices larger than four are considered exotic. The exploration of the properties of this wider class of models could prove useful in quantised gravity. Such generalisation would be in the spirit of the work done on probabilistic theories [68, 69]. Those studies often consider a diverse landscape of theories similar to quantum mechanics in order to discover why quantum mechanics, in particular, is seen in nature. Investigations of different valency spin networks could proceed along similar lines.

7 Conclusion

In this paper, we have put forward a theoretically motivated ansätze based on spin networks, a form of $SU(2)$ equivariant tensor networks. This offers a way to design $SU(2)$ equivariant variational quantum algorithms which are natural for rotationally invariant quantum systems, based on the Schur map induced by a spin-coupling diagram. Furthermore, we show that our approach leads to the same parameter spaces as generated by the twirling formula but in a direct manner that avoids the twirling computation for many-qubit gates which is highly non-trivial. For the two and three-qubit gate cases, we further justify our approach with numerical results solving the ground state problem of the $SU(2)$ symmetric Heisenberg models on the one-dimensional triangular lattice and on the Kagome lattice. Connecting to the broader literature we also show that $SU(2)$ equivariant gates are identical to the generalised permutations discussed in the context of PQC+ [26].

The connection to PQC+ is also used to argue for how our ansätze moves through a parameter space that a classical algorithm would find difficult to access. The original observation in Ref. [26] showed that the expectation value of generalised permutations in the spin-basis calculates S_n Fourier coefficients in polynomial time (a possible super-exponential speed-up) and this is now extended by our work to $SU(2)$ equivariant gates. This leads to our introduction of the term *non-classical heuristics* for quantum variational techniques which can be argued to access regions of the parameter space that are classically intractable.

It is our hope that future research in this direction can extend this notion to rigorous complexity arguments by finding a task with $SU(2)$ symmetry that is solvable by $SU(2)$ equivariant circuits where no known efficient classical algorithm exists. For example, Ref. [70] has proven quantum advantage in an ML task by designing a dataset whose classification task is convertible to the discrete logarithm problem which is efficiently solvable by a QML algorithm, yet an efficient classical algorithm is deemed impossible (unless discrete logarithm problem is in BPP). Similarly, we expect that it is possible to design an ML task related to the Fourier transformation over S_n , establishing rigorous quantum advantage arguments

in this domain as well.

Acknowledgements

RDPE and CYP contributed equally to this work. RDPE would like to acknowledge useful conversation and comments from Sergii Strelchuk, Deepak Vaid, and Pierre Martin-Dussaud. CYP thanks Seongwook Shin for helpful comments. All authors thank the Xanadu QML and software research teams at large with special thanks to Maria Schuld, David Wierichs, Joseph Bowles, and David Wakeham. This research used resources of the National Energy Research Scientific Computing Center, which is supported by the Office of Science of the U.S. Department of Energy under Contract No. DE-AC02-05CH11231.

References

- [1] Alberto Peruzzo, Jarrod McClean, Peter Shadbolt, Man-Hong Yung, Xiao-Qi Zhou, Peter J Love, Alán Aspuru-Guzik, and Jeremy L O’Brien. A variational eigenvalue solver on a photonic quantum processor. *Nat. Comm.*, 5(1):4213, 2014.
- [2] David M Blei, Alp Kucukelbir, and Jon D McAuliffe. Variational inference: A review for statisticians. *Journal of the American statistical Association*, 112(518):859–877, 2017.
- [3] Giuseppe Carleo, Ignacio Cirac, Kyle Cranmer, Laurent Daudet, Maria Schuld, Naftali Tishby, Leslie Vogt-Maranto, and Lenka Zdeborová. Machine learning and the physical sciences. *Rev. Mod. Phys.*, 91(4):045002, 2019.
- [4] Marco Cerezo, Andrew Arrasmith, Ryan Babbush, Simon C Benjamin, Suguru Endo, Keisuke Fujii, Jarrod R McClean, Kosuke Mitarai, Xiao Yuan, Lukasz Cincio, et al. Variational quantum algorithms. *Nat. Rev. Phys.*, 3(9):625–644, 2021.
- [5] David H Wolpert and William G Macready. No free lunch theorems for optimization. *IEEE Trans. Evol. Comput.*, 1(1):67–82, 1997.
- [6] Anirudh Goyal and Yoshua Bengio. Inductive biases for deep learning of higher-level cognition. *Proceedings of the Royal Society A*, 478(2266):20210068, 2022.
- [7] Taco Cohen and Max Welling. Group equivariant convolutional networks. In *International conference on machine learning*, pages 2990–2999. PMLR, 2016.
- [8] Risi Kondor and Shubhendu Trivedi. On the generalization of equivariance and convolution in neural networks to the action of compact groups. In *International Conference on Machine Learning*, pages 2747–2755. PMLR, 2018.
- [9] Michael M Bronstein, Joan Bruna, Taco Cohen, and Petar Veličković. Geometric deep learning: Grids, groups, graphs, geodesics, and gauges. *arXiv preprint arXiv:2104.13478*, 2021.
- [10] Charles R Qi, Hao Su, Kaichun Mo, and Leonidas J Guibas. Pointnet: Deep learning on point sets for 3d classification and segmentation. In *Proceedings of the IEEE conference on computer vision and pattern recognition*, pages 652–660, 2017.

- [11] Victor Garcia Satorras, Emiel Hoogetboom, and Max Welling. $E(n)$ equivariant graph neural networks. In *International conference on machine learning*, pages 9323–9332. PMLR, 2021.
- [12] David Pfau, James S Spencer, and Alexander GDG Matthews. Ab initio solution of the many-electron Schrödinger equation with deep neural networks. *Phys. Rev. Res.*, 2(3):033429, 2020.
- [13] Maria Schuld, Ilya Sinayskiy, and Francesco Petruccione. An introduction to quantum machine learning. *Contemporary Physics*, 56(2):172–185, 2015.
- [14] Marco Cerezo, Guillaume Verdon, Hsin-Yuan Huang, Lukasz Cincio, and Patrick J Coles. Challenges and opportunities in quantum machine learning. *Nat. Comp. Sci.*, 2(9):567–576, 2022.
- [15] Joseph Bowles, David Wierichs, and Chae-Yeun Park. Backpropagation scaling in parameterised quantum circuits. *arXiv preprint arXiv:2306.14962*, 2023.
- [16] Frederic Sauvage, Martin Larocca, Patrick J Coles, and Marco Cerezo. Building spatial symmetries into parameterized quantum circuits for faster training. *arXiv preprint arXiv:2207.14413*, 2022.
- [17] Maxwell West, Martin Sevir, and Muhammad Usman. Reflection equivariant quantum neural networks for enhanced image classification. *arXiv preprint arXiv:2212.00264*, 2022.
- [18] Han Zheng, Gokul Subramanian Ravi, Hanrui Wang, Kanav Setia, Frederic T Chong, and Junyu Liu. Benchmarking variational quantum circuits with permutation symmetry. *arXiv preprint arXiv:2211.12711*, 2022.
- [19] Martin Larocca, Frédéric Sauvage, Faris M Sbahi, Guillaume Verdon, Patrick J Coles, and Marco Cerezo. Group-invariant quantum machine learning. *PRX Quantum*, 3(3):030341, 2022.
- [20] Han Zheng, Zimu Li, Junyu Liu, Sergii Strelchuk, and Risi Kondor. On the super-exponential quantum speedup of equivariant quantum machine learning algorithms with $SU(d)$ symmetry. *arXiv preprint arXiv:2207.07250*, 2022.
- [21] Louis Schatzki, Martin Larocca, Frederic Sauvage, and Marco Cerezo. Theoretical guarantees for permutation-equivariant quantum neural networks. *arXiv preprint arXiv:2210.09974*, 2022.
- [22] Quynh T Nguyen, Louis Schatzki, Paolo Braccia, Michael Ragone, Patrick J Coles, Frederic Sauvage, Martin Larocca, and M Cerezo. Theory for equivariant quantum neural networks. *arXiv preprint arXiv:2210.08566*, 2022.
- [23] Andrea Skolik, Michele Cattelan, Sheir Yarkoni, Thomas Bäck, and Vedran Dunjko. Equivariant quantum circuits for learning on weighted graphs. *npj Quantum Inf.*, 9(1):47, 2023.
- [24] Johannes Jakob Meyer, Marian Mularski, Elies Gil-Fuster, Antonio Anna Mele, Francesco Arzani, Alissa Wilms, and Jens Eisert. Exploiting symmetry in variational quantum machine learning. *PRX Quantum*, 4(1):010328, 2023.
- [25] Jamie Heredge, Charles Hill, Lloyd Hollenberg, and Martin Sevir. Permutation invariant encodings for quantum machine learning with point cloud data. *arXiv preprint arXiv:2304.03601*, 2023.
- [26] Han Zheng, Zimu Li, Junyu Liu, Sergii Strelchuk, and Risi Kondor. Speeding up learning quantum states through group equivariant convolutional quantum ansätze. *PRX Quantum*, 4(2):020327, 2023.

- [27] William M Kirby and Frederick W Strauch. A practical quantum algorithm for the Schur transform. *Quantum Info. Comput.*, 18(9–10):721–742, aug 2018.
- [28] Michael Ragone, Paolo Braccia, Quynh T Nguyen, Louis Schatzki, Patrick J Coles, Frederic Sauvage, Martin Larocca, and M Cerezo. Representation theory for geometric quantum machine learning. *arXiv preprint arXiv:2210.07980*, 2022.
- [29] Joel Klassen and Barbara M Terhal. Two-local qubit hamiltonians: when are they stoquastic? *Quantum*, 3:139, 2019.
- [30] Dominik Hangleiter, Ingo Roth, Daniel Nagaj, and Jens Eisert. Easing the monte carlo sign problem. *Sci. Adv.*, 6(33):eabb8341, 2020.
- [31] Stephen P Jordan. Permutational quantum computing. *arXiv preprint arXiv:0906.2508*, 2009.
- [32] Vojtěch Havlíček and Sergii Strelchuk. Quantum Schur sampling circuits can be strongly simulated. *Phys. Rev. Lett.*, 121(6):060505, 2018.
- [33] Brian C Hall. *Lie groups, Lie algebras, and representations*. Springer Cham, 2013.
- [34] Sukhwinder Singh, Robert NC Pfeifer, and Guifré Vidal. Tensor network decompositions in the presence of a global symmetry. *Phys. Rev. A*, 82(5):050301, 2010.
- [35] Sukhwinder Singh and Guifré Vidal. Tensor network states and algorithms in the presence of a global $SU(2)$ symmetry. *Phys. Rev. B*, 86(19):195114, 2012.
- [36] Roger Penrose. Angular momentum: an approach to combinatorial space-time. *Quantum theory and beyond*, 151, 1971.
- [37] Carlo Rovelli and Lee Smolin. Spin networks and quantum gravity. *Phys. Rev. D*, 52(10):5743, 1995.
- [38] Richard DP East, Pierre Martin-Dussaud, and John Van de Wetering. Spin-networks in the ZX-calculus. *arXiv preprint arXiv:2111.03114*, 2021.
- [39] Jakub Mielczarek. Spin foam vertex amplitudes on quantum computer—preliminary results. *Universe*, 5(8):179, 2019.
- [40] Grzegorz Czelusta and Jakub Mielczarek. Quantum simulations of a qubit of space. *Phys. Rev. D*, 103(4):046001, 2021.
- [41] Grzegorz Czelusta and Jakub Mielczarek. Quantum circuits for the ising spin networks. *arXiv preprint arXiv:2304.03559*, 2023.
- [42] Vojtěch Havlíček, Sergii Strelchuk, and Kristan Temme. Classical algorithm for quantum $su(2)$ schur sampling. *Phys. Rev. A*, 99(6):062336, 2019.
- [43] Annalisa Marzuoli and Mario Rasetti. Computing spin networks. *Annals of Physics*, 318(2):345–407, 2005.
- [44] Adam Wills and Sergii Strelchuk. Generalised coupling and an elementary algorithm for the quantum Schur transform. *arXiv preprint arXiv:2305.04069*, 2023.
- [45] Dave Bacon, Isaac L Chuang, and Aram W Harrow. Efficient quantum circuits for Schur and Clebsch-Gordan transforms. *Phys. Rev. Lett.*, 97(17):170502, 2006.

- [46] Adriano Barenco, Charles H Bennett, Richard Cleve, David P DiVincenzo, Norman Margolus, Peter Shor, Tycho Sleator, John A Smolin, and Harald Weinfurter. Elementary gates for quantum computation. *Phys. Rev. A*, 52(5):3457, 1995.
- [47] Bruce E Sagan. *The symmetric group: representations, combinatorial algorithms, and symmetric functions*, volume 203. Springer New York, 2013.
- [48] Daniel A Roberts and Beni Yoshida. Chaos and complexity by design. *Journal of High Energy Physics*, 2017(4):1–64, 2017.
- [49] Nathan Jacobson. Structure theory of simple rings without finiteness assumptions. *Transactions of the American Mathematical Society*, 57(2):228–245, 1945.
- [50] Pavel I Etingof, Oleg Golberg, Sebastian Hensel, Tiankai Liu, Alex Schwendner, Dmitry Vaintrob, and Elena Yudovina. *Introduction to representation theory*, volume 59. American Mathematical Soc., 2011.
- [51] Fernando GSL Brandão, Wissam Chemissany, Nicholas Hunter-Jones, Richard Kueng, and John Preskill. Models of quantum complexity growth. *PRX Quantum*, 2(3):030316, 2021.
- [52] Y Shimizu, K Miyagawa, K Kanoda, M Maesato, and G Saito. Spin liquid state in an organic mott insulator with a triangular lattice. *Phys. Rev. Lett.*, 91(10):107001, 2003.
- [53] Ville Bergholm, Josh Izaac, Maria Schuld, Christian Gogolin, Shah Nawaz Ahmed, Vishnu Ajith, M Sohaib Alam, Guillermo Alonso-Linaje, B. Akash Narayanan, Ali Asadi, et al. PennyLane: Automatic differentiation of hybrid quantum-classical computations. *arXiv preprint arXiv:1811.04968*, 2018.
- [54] <https://github.com/PennyLaneAI/pennylane-lightning>, 2023.
- [55] <https://github.com/XanaduAI/all-you-need-is-spin>, 2023.
- [56] Sergey Bravyi, David P Divincenzo, Roberto I Oliveira, and Barbara M Terhal. The complexity of stoquastic local Hamiltonian problems. *arXiv preprint quant-ph/0606140*, 2006.
- [57] Giuseppe Carleo and Matthias Troyer. Solving the quantum many-body problem with artificial neural networks. *Science*, 355(6325):602–606, 2017.
- [58] Chae-Yeun Park and Michael J Kastoryano. Expressive power of complex-valued restricted Boltzmann machines for solving nonstoquastic hamiltonians. *Phys. Rev. B*, 106(13):134437, 2022.
- [59] Chae-Yeun Park and Nathan Killoran. Hamiltonian variational ansatz without barren plateaus. *arXiv preprint arXiv:2302.08529*, 2023.
- [60] Jan Lukas Bosse and Ashley Montanaro. Probing ground-state properties of the kagome antiferromagnetic heisenberg model using the variational quantum eigensolver. *Phys. Rev. B*, 105(9):094409, 2022.
- [61] Joris Kattemölle and Jasper Van Wezel. Variational quantum eigensolver for the Heisenberg anti-ferromagnet on the kagome lattice. *Phys. Rev. B*, 106(21):214429, 2022.
- [62] Yulan Guo, Hanyun Wang, Qingyong Hu, Hao Liu, Li Liu, and Mohammed Bennamoun. Deep learning for 3d point clouds: A survey. *IEEE Trans. Pattern Anal. Mach. Intell.*, 43(12):4338–4364, 2020.

- [63] Francesco Scazza, Christian Hofrichter, Moritz Höfer, PC De Groot, Immanuel Bloch, and Simon Fölling. Observation of two-orbital spin-exchange interactions with ultracold $SU(N)$ -symmetric fermions. *Nat. Phys.*, 10(10):779–784, 2014.
- [64] Christian Hofrichter, Luis Riegger, Francesco Scazza, Moritz Höfer, Diogo Rio Fernandes, Immanuel Bloch, and Simon Fölling. Direct probing of the mott crossover in the $SU(N)$ fermi-hubbard model. *Phys. Rev. X*, 6(2):021030, 2016.
- [65] Kasper Duivenvoorden and Thomas Quella. Discriminating string order parameter for topological phases of gapped $SU(N)$ spin chains. *Phys. Rev. B*, 86(23):235142, 2012.
- [66] Pierre Martin-Dussaud. A primer of group theory for loop quantum gravity and spin-foams. *General Relativity and Gravitation*, 51(9):1–70, 2019.
- [67] John W Barrett and Ileana Naish-Guzman. The ponzano–regge model. *Classical and Quantum Gravity*, 26(15):155014, 2009.
- [68] Michael D Mazurek, Matthew F Pusey, Kevin J Resch, and Robert W Spekkens. Experimentally bounding deviations from quantum theory in the landscape of generalized probabilistic theories. *PRX Quantum*, 2(2):020302, 2021.
- [69] Jonathan Barrett, Niel de Beaudrap, Matty J Hoban, and Ciarán M Lee. The computational landscape of general physical theories. *npj Quantum Inf.*, 5(1):41, 2019.
- [70] Yunchao Liu, Srinivasan Arunachalam, and Kristan Temme. A rigorous and robust quantum speed-up in supervised machine learning. *Nat. Phys.*, 17(9):1013–1017, 2021.
- [71] Carlo Rovelli and Francesca Vidotto. *Covariant loop quantum gravity: an elementary introduction to quantum gravity and spinfoam theory*. Cambridge University Press, 2015.
- [72] Redmond Mcnamara. Irreducible representations of the symmetric group. *Research Experience for Undergraduates*, 2013.
- [73] William Fulton and Joe Harris. *Representation theory: a first course*, volume 129. Springer Science & Business Media, 2013.

A Formal introduction to spin networks

Despite having a modest presentation, the gate architectures seen in Sec. 3 cannot be understood beyond a superficial depth without grasping the motivating concept of the spin network more deeply. The spin network can be seen as type of tensor network where the vertices are invariant under $SU(2)$ actions, and the contraction edges are indexed by irreps of $SU(2)$. This relates to a particular representation of equivariant linear maps as *harmonic tensor networks*⁹ over $SU(2)$, by which we mean a tensor network where the tensors involved are all equivariant with respect to the given group. Here however we will give the classical presentation of a spin network as a labelled graph in order to allow the interested reader to more easily follow the spin network literature.

⁹Harmonic in the sense of harmonic analysis and decomposition of functions over representations, see Ref. [66].

Labelled Directed Graphs. A spin network is a particular form of labelled directed graph. A directed graph Γ is an ordered pair $\Gamma = (\mathcal{N}, \mathcal{L})$, where $\mathcal{N} = \{n_1, \dots, n_N\}$ is a finite set of N nodes, and $\mathcal{L} = \{l_1, \dots, l_L\}$ a finite set of L edges (traditionally referred to as links in the Loop quantum gravity literature), endowed with a target map $t : \mathcal{L} \rightarrow \mathcal{N}$ and a source map $s : \mathcal{L} \rightarrow \mathcal{N}$, assigning each edge to its end and start points respectively. We denote $\mathcal{S}(n)$ (respectively $\mathcal{T}(n)$) the set of edges for which the node n is the source (respectively the target). The valency of a node n is the number of edges which have n as a endpoint, i.e., $|\mathcal{T}(n)|$. A graph is said to be p -valent if the valency of each node is p .

Intertwiners. Before defining spin networks proper by restricting ourselves to labelled directed graphs of a certain type, it will be profitable to define the concept of intertwiners. Let us say that we have two vector spaces V and W on which we have representations $U_V, U_W : G \rightarrow V$ of a group made up of elements $g \in G$ and its algebra \mathfrak{g} , an intertwiner is a linear map $T : V \rightarrow W$ which satisfies:

$$T(U_V(g) \circ v) = U_W(g) \circ T(v) \quad (80)$$

where $v \in V$. This is alternatively characterised by the commuting diagram:

$$\begin{array}{ccc} V & \xrightarrow{T} & W \\ U_V(g) \downarrow & & \downarrow U_W(g) \\ V & \xrightarrow{T} & W. \end{array} \quad (81)$$

This shows us that an intertwiner is an equivariant map. Depending on the literature this is also referred to as a covariant map.

The space of intertwiners, denoted $\text{Hom}_G(V, W)$, is a subspace of the vector space of linear maps $\text{Hom}(V, W)$ from V to W . Given a space of equivariant maps under the group G we can make the following useful identification of the *equivariant* maps with an isomorphic space of *invariant* states

$$\text{Hom}_G(V, W) \cong \text{Inv}_G(V \otimes W^*), \quad (82)$$

where W^* is the dual space of W made up of maps from W to the complex numbers. Here we define an invariant space as

$$\text{Inv}_G(E) \stackrel{\text{def}}{=} \{\psi \in E \mid \forall g \in G, g \cdot \psi = \psi\}. \quad (83)$$

We can see by the construction from G equivariant maps that the states in E when acted on by G via the representation $U_V \otimes U_W^\dagger$ must be such that for any $v \otimes w^\dagger \in V \otimes W^*$

$$(U_V \otimes U_W^\dagger)v \otimes w^\dagger = (Id \otimes U_W U_W^\dagger)v \otimes w^\dagger = v \otimes w^\dagger \quad (84)$$

which is the source of their invariance.

Let us consider again the directed graph Γ . We denote Λ_Γ by the set of labellings j that assign to any edge $l \in \mathcal{L}$ an $\text{SU}(2)$ irreducible representation characterised by the spin number $j_l \in \mathbb{N}/2$. Given a labelling $j \in \Lambda_\Gamma$, we write

$$\text{Inv}(n, j) \stackrel{\text{def}}{=} \text{Inv}_{\text{SU}(2)} \left(\bigotimes_{l \in \mathcal{S}(n)} V_{j_l} \otimes \bigotimes_{l \in \mathcal{T}(n)} V_{j_l}^* \right) \quad (85)$$

Where the V_{j_l} are the spaces of the irreps j_l associated to the edges. With this, we can now define a spin network.

spin networks. A *spin network* is a triple $\Sigma = (\Gamma, j, \iota)$, where Γ is a directed graph, with a labelling $j \in \Lambda_\Gamma$ on its edges, and a map ι that assigns to every $n \in \mathcal{N}$ an intertwiner $|l_n\rangle \in \text{Inv}(n, j)$.

Clebsch-Gordan coefficients and the vertex basis Having described the spin network abstractly it can be practical to choose a specific basis in order to look at how the vertices are represented as matrices. The smallest possible non-trivial intertwiner is three-valent, and we shall see that we can construct all larger valences from these. For the three-valent intertwiner the space is $\text{Inv}_{\text{SU}(2)}(J_{j_1} \otimes J_{j_2} \otimes J_{j_3})$ ¹⁰ and it can be given a basis by sequentially coupling the first two spins and then contracting the result with the third. Firstly we need to map the tensor product of the the first two spins $J_{j_1} \otimes J_{j_2}$ to the direct sum basis $J_{j_1} \oplus J_{j_2}$ as in

$$J_{j_1} \otimes J_{j_2} \simeq \bigoplus_{k=|j_1-j_2|}^{j_1+j_2} J_k \quad (86)$$

Here the equivalence is given by the intertwiner map:

$$\iota \left\{ \begin{array}{l} J_{j_1} \otimes J_{j_2} \rightarrow \bigoplus_{k=|j_1-j_2|}^{j_1+j_2} J_k \\ |j_1, j_2; m_1 m_2\rangle \rightarrow |km\rangle \end{array} \right. \quad (87)$$

Written like this we can see that the intertwiner map is a change of basis to one which is block diagonal. Moreover, each block is an irreducible representation. In the case when we have qubits, i.e., spin-1/2's as the first two spaces this is just the Schur map. The matrix coefficients of the map ι are given by the Clebsch-Gordan coefficients¹¹

$$C_{j_1 m_1 j_2 m_2}^{jm} := \langle j_1 m_1; j_2 m_2 | jm \rangle \quad (88)$$

Clebsch-Gordan coefficients are usually first encountered by physicists during undergraduate courses in atomic physics. They are typically presented as the obscure coefficients that dictate how different (atomic) spins states $|j_1, m_1\rangle$ and $|j_2, m_2\rangle$ combine together to form a combined $|j, m\rangle$ state as seen in the equation:

$$|jm\rangle = \sum_{m_1=-j_1}^{j_1} \sum_{m_2=-j_2}^{j_2} c_{j_1, j_2, m_1, m_2}^{jm} |j_1 m_1 j_2 m_2\rangle \quad (89)$$

where the coefficients are taken to be non-zero only when the Clebsch-Gordan conditions hold:

$$\begin{aligned} j_1 + j_2 + j &\in \mathbb{N} \\ |j_1 - j_2| &\leq j \leq j_1 + j_2. \end{aligned} \quad (90)$$

It is notable that the space $\text{Inv}_{\text{SU}(2)}(J_{j_1} \otimes J_{j_2} \otimes J_{j_3})$ is one dimensional, meaning there is only one intertwiner up to a scalar. This makes sense because in the three-valent case the choice of two spins is completely fixes the third [66].

¹⁰Note we have dropped the reference to the last space being the conjugate, this is common in the literature as they are isomorphic.

¹¹In the spin network literature we often see that vertices described via Wigner symbols instead of Clebsch-Gordan coefficients as seen here. The Wigner symbols are an equivalent way to decompose three vector spaces as is done here that is more symmetric, since we are looking to derive computations with a well defined input and output it is simpler for us to use this basis instead. See Ref. [38] for more details.

For higher valence networks we can build a similar basis by reapplying the decomposition procedure seen in Eq. (86) until all the tensor products are replaced by direct sums. For example in the case of four-valent spin networks we reapply Eq. (86) to three-valent product spaces tensored with the third spin

$$\left(\bigoplus_{k=|j_1-j_2|}^{j_1+j_2} J_k \right) \otimes J_{j_3} = \bigoplus_{j_{12}=|j_1-j_2|}^{j_1+j_2} \bigoplus_{k=|j_{12}-j_3|}^{j_{12}+j_3} J_k. \quad (91)$$

This in terms of states and Clebsch-Gordan coefficients leads to the following:

$$|(j_1 j_2) j_3; j_{12} kn\rangle = \sum_{m_1, m_2, m_3, m_{12}} C_{j_1 m_1 j_2 m_2}^{j_{12} m_{12}} C_{j_{12} m_{12} j_3 m_3}^{kn} \bigotimes_{i=1}^3 |j_i, m_i\rangle. \quad (92)$$

It is important to note that there is a freedom in the ordering of the breakdown of a tensor product of three elements into direct sums. Here we take the first two spins, consider the resultant direct sum, and then take the tensor product with the third space. This could be reversed and we could take the second and third or indeed the first and third. These separate decompositions amount to different basis choices which play a role in the structure of permutational quantum computing discussed above (see Sec. 6). The quantum gravity community is mostly interested in three- and four-valent spin networks due to a relationship with 2D and 3D space models of gravity (see further below in this section and Refs. [71, 66]). Our interests are in principle broader than this though all spin networks can be decomposed into three-valent ones. In addition, there is also a direct relationship with the present quantum computing literature and three-valent intertwiners due to the work on PQC.

B The representation theory of the symmetric group

In this Appendix, we briefly introduce the irreducible representation of the symmetric group S_n .

Consider a partition of a positive integer n to be a monotonically decreasing sequence of positive integers, $\lambda = (\lambda_1, \lambda_2, \dots)$ that sum to n . We can associate these with cycle shapes of S_n . For example given 10 elements we can associate the partition $\lambda = (4, 2, 2, 2)$ with a permutation decomposable into one four-cycle and three two-cycles.

A Young diagram is a diagrammatic depiction of the cycle shapes of S_n . Typically the largest cycle goes at the top and for every element in the cycle we add a box as seen here:


(93)

A *Standard filling* of a Young diagram is an bijective map of the numbers from 1 to n , where n is the number of boxes such that the entries increase along the rows and down the columns. The standard filled Young diagram is called a *Young tableau*

$$\begin{array}{|c|c|c|c|}
\hline
1 & 3 & 4 & 7 \\
\hline
2 & 8 & & \\
\hline
5 & 9 & & \\
\hline
6 & 10 & & \\
\hline
\end{array} \tag{94}$$

We can act with an element of the symmetric group on the tableau by simply applying the permutation $\alpha \in S_n$ to the filling numbers.

Let us define the equivalence class $R(T)$ of permutations that only move elements about *within their rows*. In this way we define the row stabilisers which are simply the product subgroups $\bigotimes_{p \in \lambda} S_p$. In our earlier example it would be the space $S_4 \otimes S_2 \otimes S_2 \otimes S_2$. In an analogous fashion we can also describe the column stabilisers $C(T)$.

To describe the irreps of S_n we will need the Young polytabloid:

$$e_T = \{T\} = \sum_{\alpha \in C(T)} \text{sgn}(\alpha) \alpha \triangleright T \tag{95}$$

where $\text{sgn}(\alpha)$ is the parity function giving 1 for an even permutation or -1 for an odd one. We note that that $\alpha \triangleright T$ is not necessarily itself a Young tableau due to its non-standard filling.

For example given the tableau

$$\begin{array}{|c|c|}
\hline
1 & 2 \\
\hline
3 & \\
\hline
\end{array} \tag{96}$$

the polytabloid is given by

$$\left\{ \begin{array}{|c|c|} \hline 1 & 2 \\ \hline 3 & \\ \hline \end{array} \right\} = \text{sgn}(Id) \begin{array}{|c|c|} \hline 1 & 2 \\ \hline 3 & \\ \hline \end{array} + \text{sgn}((1,3)) \begin{array}{|c|c|} \hline 3 & 2 \\ \hline 1 & \\ \hline \end{array} = \begin{array}{|c|c|} \hline 1 & 2 \\ \hline 3 & \\ \hline \end{array} - \begin{array}{|c|c|} \hline 3 & 2 \\ \hline 1 & \\ \hline \end{array} \tag{97}$$

A Specht module is a module¹² spanned by polytabloids e_T where T is the index corresponding to all tableaux of shape λ . That is to say,

$$Sp^{(\lambda)} = \{c_1 e_{T_1} + c_2 e_{T_2} + c_3 e_{T_3} + \dots \mid c_1, c_2 \dots \in \mathbb{C} \text{ and } T_1, T_2 \dots \text{ are tableaux of shape } \lambda\}. \tag{98}$$

It can be shown that the Specht modules are the irreps of S_n [72].

In the context of the above work let $n = 3$, and restrict to the Young diagrams with at most two rows which correspond to the multiplicity of elements of $SU(2)$ by Schur-Weyl duality. These are

$$\begin{array}{|c|c|c|}
\hline
& & \\
\hline
\end{array} \quad \text{and} \quad \begin{array}{|c|c|}
\hline
& \\
\hline
& \\
\hline
\end{array}. \tag{99}$$

The irreducible representations of S_3 associated with the first diagram is dimension 1 and the second diagram is dimension 2. More precisely, the Specht module for the first diagram is generated by a single vector

¹²A generalisation of a vector space. A vector space has scalars belonging to a field but a module has scalars that are merely from a ring (meaning the multiplicative operation does not have to be a commutative group). Though we range over the field \mathbb{C} in our example this is not generally the case hence the literature using the term module.

$$\{\boxed{1}\boxed{2}\boxed{3}\} = \boxed{1}\boxed{2}\boxed{3}. \quad (100)$$

for the second diagram it is generated by two vectors which correspond to the two possible tableau

$$\left\{ \begin{array}{|c|c|} \hline \boxed{1} & \boxed{3} \\ \hline \boxed{2} & \\ \hline \end{array} \right\} = \begin{array}{|c|c|} \hline \boxed{1} & \boxed{3} \\ \hline \boxed{2} & \\ \hline \end{array} + \begin{array}{|c|c|} \hline \boxed{2} & \boxed{3} \\ \hline \boxed{1} & \\ \hline \end{array} \quad (101)$$

and

$$\left\{ \begin{array}{|c|c|} \hline \boxed{1} & \boxed{2} \\ \hline \boxed{3} & \\ \hline \end{array} \right\} = \begin{array}{|c|c|} \hline \boxed{1} & \boxed{2} \\ \hline \boxed{3} & \\ \hline \end{array} - \begin{array}{|c|c|} \hline \boxed{3} & \boxed{2} \\ \hline \boxed{1} & \\ \hline \end{array} \quad (102)$$

Referring back to the Schur-Weyl decomposition where the irreps of S_n give the multiplicities of the $SU(2)$ irreps, we observe:

$$(\mathbb{C}^2)^{\otimes 3} \simeq J_{3/2} \oplus 2J_{1/2}, \quad (103)$$

as the three row element corresponds to the fully symmetric subspace of the three qubit components, i.e., $\text{spin-}\frac{3}{2}$ and the mixed representation corresponds to the $\text{spin-}\frac{1}{2}$. For more details see Refs. [47, 73].

C LQG, quantised geometry, and the geometry of $SU(2)$ equivariant algorithms

C.1 What is LQG?

In this appendix, we refer to the work done in Ref. [71] for more details. Loop quantum gravity (LQG) is based on the idea that space-time is quantised, and it describes space using a Hilbert space whose basis is indexed by *spin networks*. These spin networks can be seen as the dual space of tessellating simplices, such as triangles in 2+1 dimensions or tetrahedra in 3+1 dimensions. Length, angle, area, and volume operators act on these spin networks, yielding quantised answers. The dynamics of LQG are described by spinfoams, which can be viewed as maps between spin networks. Spinfoams are the fundamental objects, and spin networks can be seen as particular foliations of the spinfoams, where each ‘moment’ is a superposition of states of quantised space represented by the spin networks. The transition amplitudes are obtained by summing over all spinfoams that are bounded by the initial and final spin networks that are being transitioned between.

LQG’s historical development has been involved, and although more elegant routes to LQG may emerge if the theory proves successful, we currently rely on the present understanding. Given the theory’s novelty to some readers, we provide a brief outline of how one arrives at spin networks and spinfoams. General relativity is typically modeled by a manifold \mathcal{M} with a metric $g_{\mu\nu}$ that varies from point to point. To quantise gravity via second quantization, a time parameter is needed. This can be achieved by ADM splitting [71], which divides the space into 3D foliations Σ_t indexed by $t \in \mathbb{R}$, making space-time a product of Σ and \mathbb{R} . The classical configuration space \mathcal{C} is defined by possible metrics q_{ab} on 3D foliations Σ_t , and the Einstein equations govern how we move from one slice with metric q_{ab} to another. One can go on to define an extrinsic curvature k_{ab} which defines a ‘momentum’ on Σ_0 . Together with q_{ab} they describe a classical state of space-time and define a point in the phase space \mathcal{P} .

Diffeomorphism invariance imposes constraints on the phase space, indicating that only a subspace of \mathcal{P} is needed to describe physical states. To quantise, we move from phase space \mathcal{P} to a Hilbert space \mathcal{H} , and the coordinates of \mathcal{P} become operators on \mathcal{H} . Though it should be noted on the way Ashtekar-Barbero variables (A_i^a, E_a^i) are used instead of (q_{ab}, k_{ab}) , which brings general relativity closer to successfully quantised gauge theories. Truncation is performed by taking a finite graph Γ embedded within Σ , reducing the phase space from 3D to 1D. Holonomies along the links of Γ are used to describe the relevant parts of the phase-space, resulting in a finite-dimensional space. The Hilbert space \mathcal{H}_Γ is a space of square-integrable functions of the holonomies.

There are other constraints in LQG, notably the Gauss constraint, which restricts the Hilbert space to the invariant subspaces. This in turn leads to the final Hilbert space in LQG being a sum over all possible $SU(2)$ invariant graphs, where each graph represents a spin network with an edge label as irreducible representations of $SU(2)$ and vertices as intertwiners of the attached edges. These spin networks then form a basis for describing quantum states of space in LQG, and indeed, as is discussed below, they have an interpretation in terms of quantised shapes with appropriate operators.

C.2 Seeing geometry in spin networks

It is possible to view $SU(2)$ coupling theory, typically understood through the arcane use of Clebsch-Gordan coefficients or alternatively by Wigner or Racah symbols, as statements about geometries with quantised values. While this approach is presently unusual it is more intuitive. This is the source of the geometric interpretation of spin networks.

The quantised triangle perspective The Clebsch-Gordan conditions are more interesting than they appear. Consider them once more:

$$\begin{aligned} j_1 + j_2 + j &\in \mathbb{N} \\ |j_1 - j_2| &\leq j \leq j_1 + j_2. \end{aligned} \tag{104}$$

The reason they are more interesting than they seem at first sight is hinted at by the specific name for the second of these constraints. It is known as the *triangle inequality*. Given a triangle with sides with lengths that we will suggestively label j, j_1 and j_2 , which are in $\frac{\mathbb{N}}{2}$, it is an elementary fact that the length j in a valid triangle must be smaller than or equal to the combined lengths of the other sides and larger than the magnitude of the difference of the other edges¹³. This invites the interpretation of non-zero spin-coupling coefficients as indicating the existence of valid triangles with spin magnitude edge lengths. The first condition is a little more mysterious. The condition that the three half-integers sum to a whole number implicitly requires that the number of summed $\frac{1}{2}$'s is even. If we recall however that spin- $\frac{n}{2}$ is the symmetric subspace of n copies of spin- $\frac{1}{2}$ we can interpret this as demanding that, when decomposed into spin- $\frac{1}{2}$ components, there are enough spin- $\frac{1}{2}$'s to be paired up. This perspective is further justified in that both conditions can be rewritten as $2j_1 = b+c, 2j_2 = c+a, 2j_3 = a+b$ for three non-negative integers a, b , and c . This permits us to understand both conditions in terms of the picture seen in Fig. 12 which matches these conditions on triangles to the ability to bring three half integer spins together (broken down into spin- $\frac{1}{2}$ components). This observation was first outlined in Penrose's binor calculus which offered a way to decompose spin networks into (the symmetric subspace of) spin- $\frac{1}{2}$

¹³The that we discretise in terms of values of $\frac{1}{2}$ is more a feature of measurement outcomes for spin, the mathematicians index $SU(2)$ by integers without much difficulty.

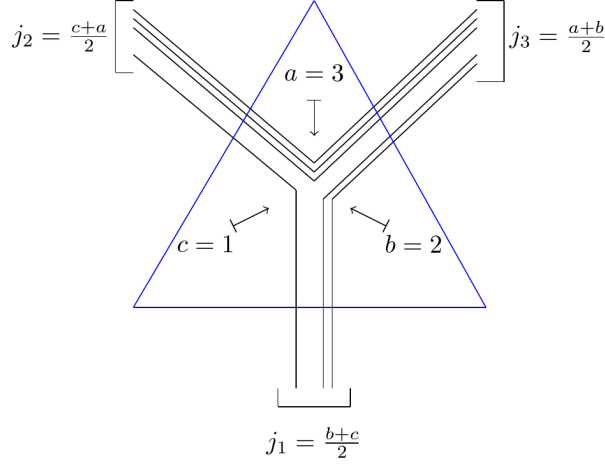


Figure 12: Relationship between the CG coefficients for discretised edge lengths and the non-negative integers a, b , and c . We can see these as indicating pairings of a decomposition of the edge lengths in amounts of $\frac{1}{2}$ [71].

wires meeting at vertices which correspond to their coupling [36]. These binor calculus diagrams can also be viewed as a type of spin network and have previously been converted into a form close to qubit quantum computing via the ZX calculus [38].

At this point we have an interpretation of coupling spins as relating to the existence of valid triangles with edges determined by the spins involved. However, to see a ‘quantised geometry’ of triangles we require both states and operators: the former being mathematical objects from which the latter can meaningfully extract eigenvalues that correspond to geometric properties. For a triangle these are length and area. Consider two spins coupling to third, the triangle inequality tells us that if we took the size of the input spins as edges of a triangle the possible output spins are exactly those that could complete the triangle. A practical, and importantly generalisable, perspective is to take the three spins as vectors lying dual to the triangle, which we can do since the spin-values obey the triangle inequality, where we note that they will be such that $\sum \vec{j}_i = 0$. When we look at the intertwiner space $\text{Inv}_{\text{SU}(2)}(\mathcal{H}_{j_1} \otimes \mathcal{H}_{j_2} \otimes \mathcal{H}_{j_3}^*)$ where each space corresponds to a spin j , we can see this is characterised by a single triangle whose edges lie dual to the spins whose size is dictated by the given spin’s magnitudes. The length operator gives us the quantised lengths of the edges of this triangle and is simply the angular momentum operator \vec{J} acting on any of the spins to give $\sqrt{j(j+1)}$. Furthermore for an area operator we can use $\vec{A} = \frac{1}{2} \vec{j}_1 \wedge \vec{j}_2$ ¹⁴. In line with this, in the case of a three-valent spin network when intertwiners share an edge they can be seen as sharing a length of the associated triangle rendering the entire spin network a tessellating geometry of quantised triangles.

Quantised tetrahedra Let us now consider a tetrahedra and proceed in the manner of Ref. [71]. It is a shape composed of 4 triangular faces whose edges are constrained by virtue of coming together to form this shape. It can be usefully characterised by 4 dual vectors $\vec{J}_a, a = 1, \dots, 4$ lying orthogonal to each face. We say that each $\vec{J}_a = \frac{1}{2} \vec{e}_1 \wedge \vec{e}_2$ where \vec{e}_i are the vectors chosen to represent two of the edges

¹⁴ $\vec{a} \wedge \vec{b} = \|\vec{a}\| \|\vec{b}\| \sin(\theta) \frac{\vec{n}}{\|\vec{n}\|}$ where \vec{n} is the vector normal to the plane defined by \vec{a} and \vec{b} oriented by the right-hand-rule/cross product convention.

of the triangle whose face lies orthogonal to \vec{J}_a . Note how by definition \vec{J}_a lies normal to the faces of the tetrahedra. Let us take these \vec{J}_a to literally be spins, this implies that we have the commutation relation

$$[J^i, J^j] = i\hbar \varepsilon^{ij}_k J^k. \quad (105)$$

Moreover as the magnitude of the spins correspond to the faces we quantify their area as

$$A = \sqrt{j(j+1)}, \quad j = 0, \frac{1}{2}, 1, \frac{3}{2}, 2, \dots \quad (106)$$

(in general the total angular momentum operator gives the n-1 simplex magnitude of your n-simplex, hence it was length in the triangle case). In this way every face of the tetrahedra has an area given by their magnitude¹⁵. One can further show that the following property holds

$$\vec{C} := \sum_{a=1}^4 \vec{J}_a = 0 \quad (107)$$

which is the same condition as seen in the triangular case (again this persists in higher dimensions). One can also note that the (oriented) volume¹⁶ is given by

$$V^2 = \frac{2}{9} \vec{J}_1 \wedge \vec{J}_2 \wedge \vec{J}_3 = \frac{2}{9} (\vec{J}_1 \times \vec{J}_2) \cdot \vec{J}_3 = \frac{2}{9} \epsilon_{ijk} J_1^i J_2^j J_3^k = \frac{2}{9} \det J. \quad (108)$$

The condition in Eq. (107) is crucial because it indicates we can restrict the space in which these quantised tetrahedra live from the Hilbert space $H = H_{j_1} \otimes H_{j_2} \otimes H_{j_3} \otimes H_{j_4}$ to where $\vec{C} = 0$ i.e. $\text{Inv}_{\text{SU}(2)}[H_{j_1} \otimes H_{j_2} \otimes H_{j_3} \otimes H_{j_4}]$. Formally one can show that the closure condition is invariant under the action of an $\text{SU}(2)$ rotation [66]. Geometrically we can get a feeling for this from recalling that $\text{SU}(2)$ is essentially $\text{SO}(3)$ (i.e., the space of rotations) contracted under the fact that only rays in Hilbert space are physically meaningful. With this in mind consider that each vector gives the size and position of a triangular face. In general these vectors could point in any direction but we are restricted to a tetrahedra. Why is this the case? Well we can see that in the tetrahedral case if we move any face relative to the others then the vectors will no longer sum to zero. They all have to be rotated together, much like rotating the whole tetrahedra. Here however we are looking at quantised spins and so rotations are defined up to rays in Hilbert space so the rotation group that is really of interest is $\text{SU}(2)$. This tells us that our tetrahedral volumes just live in $\text{Inv}_{\text{SU}(2)}[H_{j_1} \otimes H_{j_2} \otimes H_{j_3} \otimes H_{j_4}]$. This principle of invariant volumes tied to vectors summing to zero generalises to arbitrary simplices and tells us that there is a quantised geometric perspective for all dimensions. Interestingly they can all be reduced back to the three-valent case.

Triangle decomposition The space $\text{Inv}_{\text{SU}(2)}[H_{j_1} \otimes H_{j_2} \otimes H_{j_3} \otimes H_{j_4}]$ can be broken down into two invariant spaces of three Hilbert spaces. There is some freedom in how they are partitioned but the composite spaces will resemble $\text{Inv}_{\text{SU}(2)}[H_{j_1} \otimes H_{j_2} \otimes H_j^*]$ and $\text{Inv}_{\text{SU}(2)}[H_j \otimes H_{j_3}^* \otimes H_{j_4}^*]$. To see this we can look to Eq.(92) which we can apply twice in this case to give

$$((j_1 j_2) j_3) j_4; j k l m = \sum_{m_1, m_2, m_3, m, n, m_4}^{j m} C_{j_1 m_1 j_2 m_2}^{j m} C_{j m_1 m_3, m_3}^{k m} C_{k \pi i_4, m_4}^{l m} \times \bigotimes_{i=1}^4 (j_i, m_i) \quad (109)$$

¹⁵As the vector product of two vectors gives the area of the parallelogram they form, halving this gives that of the triangle.

¹⁶We have suppressed the natural magnitude units of \hbar .

$$\begin{aligned}
& \text{Inv}_{\text{SU}(2)}(H^2 \otimes H^2 \otimes H^2 \otimes H^2) = \text{Diagram of a tetrahedron with four external edges} \\
& = \text{Span} \left[\begin{array}{cc} |J=1\rangle\langle J=1| = \text{Diagram of a tetrahedron with internal edge labeled 1} & , \quad |J=0\rangle\langle J=0| = \text{Diagram of a tetrahedron with internal edge labeled 0} \end{array} \right]
\end{aligned}$$

Figure 13: The vertices are the invariant space of four spin- $\frac{1}{2}$ s, $\text{Inv}_{\text{SU}(2)}(J_{1/2} \otimes J_{1/2} \otimes J_{1/2} \otimes J_{1/2})$, which written in the form of Eq. (11). In the LQG literature the invariant space of 4 spins is often depicted as a tetrahedra to which this space corresponds when seen in terms of quantised geometry. More conventionally we can see that this space is spanned by the $J = 0$ and $J = 1$ irrep spaces (which have different dimensions). We also show how these subspaces can be represented as tensor networks corresponding to the two ways one can combine the input and output spaces. The triangles correspond to the decomposition of the 4-valent vertex into two three-valent spaces which are viewed as quantised triangles. In our four-valent spin networks circuits we are directly parameterising these two possible composing triangle geometries for each vertex which we interpret as a tetrahedra.

where $j \in \{|j_1 - j_2|, \dots, j_1 + j_2\}$, $k \in \{|j - j_3|, \dots, j + j_3\}$, $l \in \{|k - j_4|, \dots, k + j_4\}$, and $n \in \{-l, \dots, l\}$, which can be shown to form an orthonormal basis of the space [66]. The crucial part to notice here is that this space is formed by two trivalent spaces with one of the spin spaces summed over (for a more thorough and diagrammatic explanation of this see Ref. [38] or Ref. [66]). The external spins are fixed but the internal space that is summed over points to a particular basis decomposition of the tetrahedra into two pairs of triangles with the different j values at their intersection. For instance let us consider the invariant space of 4 spins. We can deduce that as it is composed of two three-valent invariant spaces, both of which have two components which are spin- $\frac{1}{2}$, they will be decomposed into the case where the internal spin space is $j = 0$ or $j = 1$. Pictorially this is represented in Fig. 13. This principle generalises and with larger invariant spaces we get higher order n -simplices (where a triangle is a two-simplex, a tetrahedra a three-simplex etc) that decompose into $n - 1$ triangles with $n - 2$ interior edges that give the different possible values which in turn give a possible triangular basis.

C.3 SU(2) equivariant algorithms as the search for optimal triangulations

In short, the geometric approach gives the structure of SU(2) equivariant algorithms a distinctly geometric flavour. Consider that our parameterised spin networks have the specific property that the parameterisation does not alter the input or output space itself meaning that they can be seen as the optimisation of transition maps between $n - 1$ simplices (which are the surface of the n -simplex corresponding to the spin-network circuit). In our four-valent example, we can consider the spin networks as quantised tetrahedra or, by flattening this perspective, collections of two triangles whose internal edge lengths correspond to the different internal intertwiner bases elements as seen in Fig. 13.

It is possible to take this geometric perspective further still. We can view our spin networks as maps between quantised 2D spaces in line with Jordan [31]. This presents an interesting perspective

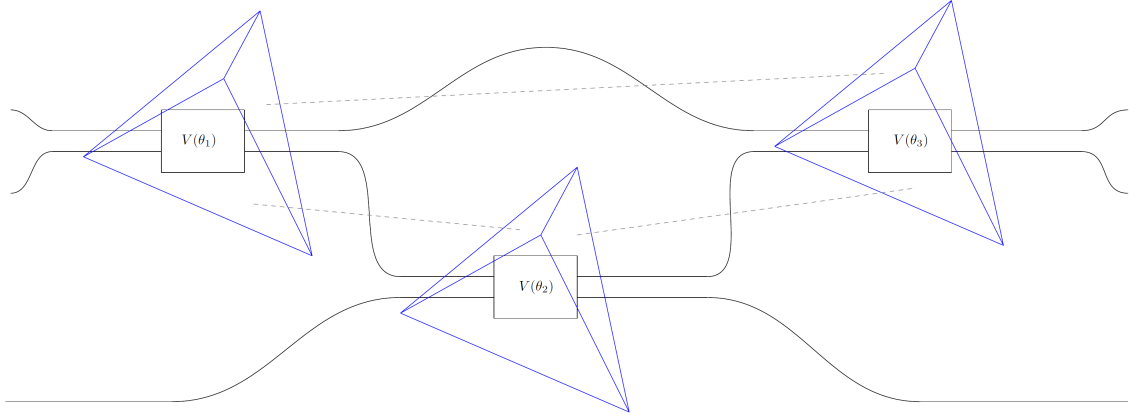


Figure 14: A spin-network circuit with a representation of the three quantised tetrahedra that lie dual to each vertex. Each of their faces has an area of $\frac{\sqrt{3}}{2}\hbar$ which is the total angular momentum of a qubit. The dotted grey lines indicate the faces shared by the tetrahedra that correspond to the qubits passing from the output of one gate to the input of the other. From the perspective of our 4-valent spin-network circuits (the 2 qubit vertex gates) our variational algorithm is an optimisation of these tessellating tetrahedra (or 5-simplices for the three-qubit vertex gate).

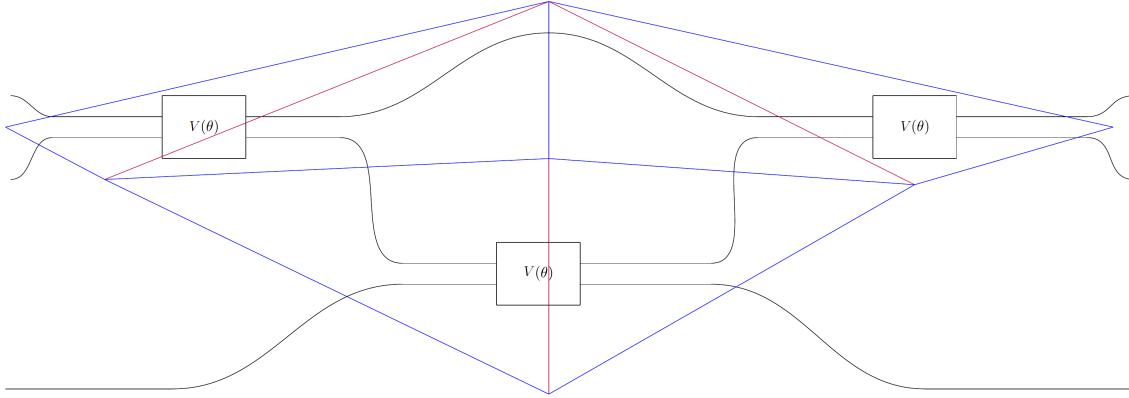


Figure 15: The triangulated interpretation of the spin-network circuit seen as tetrahedra above in Fig. 14. The three tetrahedra have been decomposed into two triangles each where the exterior edge lengths are fixed at $\frac{\sqrt{3}}{2}\hbar$. The internal red edge, as determined by the intertwiner basis for the tetrahedra, is either 0 or $\sqrt{2}$ which are the eigenvalues for the total angular momentum operator of the internal edge as seen in Eq. (106). The phases associated to the different possible measurement lengths for the red edges are the trainable parameters in this network.

of parameterised spin networks as a restricted variety of quantised path integrals. To understand this statement we should first revisit the concept of a spinfoams [71]. In LQG where we have (four-valent) spin networks as a basis of the states of quantised 3D space the spinfoams are the maps between these states. They can be viewed as four-simplices whose boundaries are the collections of tetrahedra that make up the initial and final state geometries. They are the discretised equivalent of a particular path in the path integral approach to state transition in that there is a function that acts on them that allows for the computation of an amplitude, and the sum over all possible amplitudes gives you the probability of moving from the initial state, i.e. from the faces at one side of the 4-simplex to the final state which are the faces at the other.

This requires that the input and output spaces are fixed in order for it to make sense from the transition amplitude perspective of sending one set of simplices to another, however, as said above, this is exactly what we have for our trainable spin networks. Consider our four-valent spin-network circuits for example, which are formed of tetrahedra and so in this perspective can be viewed as 3D spinfoams. On one side we can see there are the qubits passing into the circuit which can be interpreted as dual to the triangles of tetrahedra. On the other side, the outputs also determine the triangles dual to tetrahedra. We can see then that the specific spin-network circuit is a discretisation of a specific transition path for 2D quantised geometry (because it only uses tetrahedra of a certain size connected in the way specified by the gates, a more general representation would have to remove these restrictions). Looking more broadly at circuits with arbitrary vertex sizes, these amount to collections of simplices of dimensions ranging from 3 to n , with the same restriction that their $n - 1$ faces are of size $\sqrt{2}$ (as qubits) and that their connective topology is fixed. These correspond to a more general class of n degree spinfoams, though one should note that even in the extreme case of one single n -qubit vertex gate, that in principle runs over every compatible triangle decomposition, it is still premised on a fixed number of internal vertices. The true spin-foam transition amplitude sums over all possibilities which would include an infinite number of possible internal vertices (naturally in practice a normalisation parameter is expected to ensure we arrive at a finite value).

Whatever the order of the $n - \text{degree}$ of the spinfoam we ultimately use, the optimisation algorithms of our equivariant circuits amount the optimisation of the internal parameterisation of the simplices that make up the transition amplitude. As we have seen above, these can always be decomposed into different tessellations of triangles. Choosing a specific parameter for a vertex gate then amounts to choosing a specific superposition of these internal tessellations with the connective structure of the circuit detailing how these internal tessellations are connected to each other. Though unusual, this is clearly a radically geometric interpretation of $SU(2)$ equivariant algorithms and it would be interesting to know if this kind of ‘geometerisation’ generalises to other groups.

D Further notes on the Schur gate

Equivariance of the Schur gate Focusing on the Schur matrix in Eq. (13), a natural question to ask is: How are the representations of the group acting on the input affected by the Schur map? As discussed, the input space has the tensor product representation and the output has the spin representation, which function differently. A useful shorthand to express the idea of a group element g acting on some space H without worrying about how exactly it is represented is to write $g \triangleright H$. With this in mind let us consider the action of $SU(2)$ for the two qubit case, for an arbitrary element $g \in SU(2)$, the input space of the Schur map will transform as $g \triangleright (\mathbb{C}^2 \otimes \mathbb{C}^2) = (g \triangleright \mathbb{C}^2) \otimes (g \triangleright \mathbb{C}^2) = U_g \otimes U_g$, where U_g

is the qubit representation of the element g . The output space however will transform differently as we are viewing the space as composed of spin components, $g \triangleright (J^0 \oplus J^1) = (g \triangleright J^0) \oplus (g \triangleright J^1) = J^0 \oplus (g \triangleright J^1) = Id \oplus \pi^1(g)$, where we note that the action on the single element spin-0 subspace is trivial and $\pi^1(g)$ is the spin-1 representation of the element g . We can use the Schur map itself as a mapping between the tensor product basis and the spin space to create a representation on the direct product, i.e., $U(g)^{\otimes k} = S^\dagger \pi(g) S$, which we can see as mapping our tensor space to the spin-space, performing the group action there, and then sending it back. Let us now see if our Schur map S is equivariant under the action of g , it is a direct and short calculation

$$S_2(Id \oplus \pi^1(g)) = S_2(S_2^\dagger U(g)^{\otimes k} S_2) = U_g^{\otimes k} S_2 \quad (110)$$

The group action has moved from the right hand side of the Schur gate to the left and so commutes, which is the definition of equivariance. This calculation though short can be somewhat deceptive, it is imperative that we remember that the action of the group should be represented differently before and after the Schur gate. The effect of placing the group action between the Schur gates was to transform it to the appropriate action on the spin space.

A similar discussion applies to the the three qubit space. Recalling that $\mathbb{C}^2 \otimes \mathbb{C}^2 \otimes \mathbb{C}^2 \simeq J^{\frac{1}{2}} \oplus J^{\frac{1}{2}} \oplus J^{\frac{3}{2}}$ we would then say that $g \in G$ acts as $g \triangleright (J^{\frac{1}{2}} \oplus J^{\frac{1}{2}} \oplus J^{\frac{3}{2}}) = (g \triangleright J^{\frac{1}{2}}) \oplus (g \triangleright J^{\frac{1}{2}}) \oplus (g \triangleright J^{\frac{3}{2}})$ and in the end we have that we can use the Schur gate to map us between representations acting on these spaces:

$$S_3(\pi^{\frac{1}{2}}(g) \oplus \pi^{\frac{1}{2}} \oplus \pi^{\frac{3}{2}}(g)) = S_3(S_3^\dagger U(g)^{\otimes k} S_3) = U(g)^{\otimes k} S_3. \quad (111)$$

Indeed this structure will hold in general.

The Schur gate and PQC recoupling diagrams As elements of the spin-basis, the PQC diagrams exactly correspond to the elements of the Schur basis. When specific J_z values are fixed on all the external wires, one can use the PQC diagrams to index the Schur matrix:

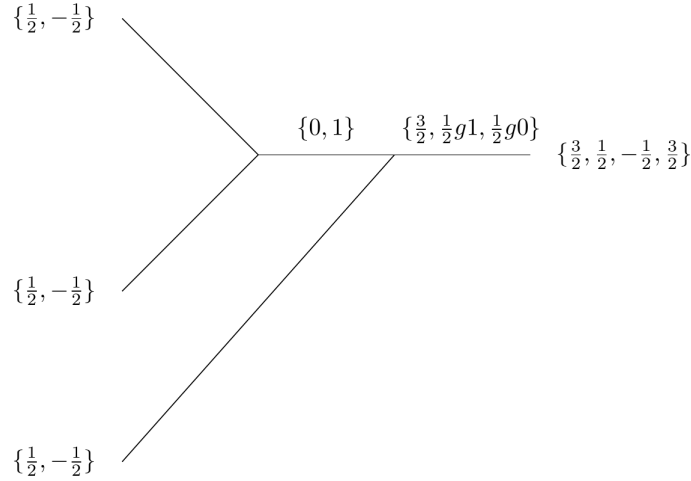
$$S_2 = \begin{pmatrix} 1 & 0 & 0 & 0 \\ 0 & \frac{1}{\sqrt{2}} & \frac{1}{\sqrt{2}} & 0 \\ 0 & 0 & 0 & 1 \\ 0 & \frac{1}{\sqrt{2}} & -\frac{1}{\sqrt{2}} & 0 \end{pmatrix} = \begin{pmatrix} c_{\frac{1}{2}, \frac{1}{2}, \frac{1}{2}, \frac{1}{2}}^{1,1} & c_{\frac{1}{2}, \frac{1}{2}, \frac{1}{2}, -\frac{1}{2}}^{1,1} & c_{\frac{1}{2}, -\frac{1}{2}, \frac{1}{2}, \frac{1}{2}}^{1,1} & c_{\frac{1}{2}, -\frac{1}{2}, \frac{1}{2}, -\frac{1}{2}}^{1,1} \\ c_{\frac{1}{2}, \frac{1}{2}, \frac{1}{2}, \frac{1}{2}}^{1,0} & c_{\frac{1}{2}, \frac{1}{2}, \frac{1}{2}, -\frac{1}{2}}^{1,0} & c_{\frac{1}{2}, -\frac{1}{2}, \frac{1}{2}, \frac{1}{2}}^{1,0} & c_{\frac{1}{2}, -\frac{1}{2}, \frac{1}{2}, -\frac{1}{2}}^{1,0} \\ c_{\frac{1}{2}, \frac{1}{2}, \frac{1}{2}, \frac{1}{2}}^{1,-1} & c_{\frac{1}{2}, \frac{1}{2}, \frac{1}{2}, -\frac{1}{2}}^{1,-1} & c_{\frac{1}{2}, -\frac{1}{2}, \frac{1}{2}, \frac{1}{2}}^{1,-1} & c_{\frac{1}{2}, -\frac{1}{2}, \frac{1}{2}, -\frac{1}{2}}^{1,-1} \\ c_{\frac{1}{2}, \frac{1}{2}, \frac{1}{2}, \frac{1}{2}}^{0,0} & c_{\frac{1}{2}, \frac{1}{2}, \frac{1}{2}, -\frac{1}{2}}^{0,0} & c_{\frac{1}{2}, -\frac{1}{2}, \frac{1}{2}, \frac{1}{2}}^{0,0} & c_{\frac{1}{2}, -\frac{1}{2}, \frac{1}{2}, -\frac{1}{2}}^{0,0} \end{pmatrix} =$$

$$\left(\begin{array}{cccc}
\begin{array}{c} \frac{1}{2} \\ \diagdown \end{array} \begin{array}{c} 1 \\ \diagup \end{array} & \begin{array}{c} \frac{1}{2} \\ \diagdown \end{array} \begin{array}{c} 1 \\ \diagup \end{array} & \begin{array}{c} \frac{1}{2} \\ \diagdown \end{array} \begin{array}{c} 1 \\ \diagup \end{array} & \begin{array}{c} \frac{1}{2} \\ \diagdown \end{array} \begin{array}{c} 1 \\ \diagup \end{array} \\
1;1 & 1;1 & 1;1 & 1;1 \\
\begin{array}{c} -\frac{1}{2} \\ \diagdown \end{array} \begin{array}{c} 1 \\ \diagup \end{array} & \begin{array}{c} -\frac{1}{2} \\ \diagdown \end{array} \begin{array}{c} 1 \\ \diagup \end{array} & \begin{array}{c} -\frac{1}{2} \\ \diagdown \end{array} \begin{array}{c} 1 \\ \diagup \end{array} & \begin{array}{c} -\frac{1}{2} \\ \diagdown \end{array} \begin{array}{c} 1 \\ \diagup \end{array} \\
1;0 & 1;0 & 1;0 & 1;0 \\
\begin{array}{c} -\frac{1}{2} \\ \diagdown \end{array} \begin{array}{c} 1 \\ \diagup \end{array} & \begin{array}{c} -\frac{1}{2} \\ \diagdown \end{array} \begin{array}{c} 1 \\ \diagup \end{array} & \begin{array}{c} -\frac{1}{2} \\ \diagdown \end{array} \begin{array}{c} 1 \\ \diagup \end{array} & \begin{array}{c} -\frac{1}{2} \\ \diagdown \end{array} \begin{array}{c} 1 \\ \diagup \end{array} \\
1;-1 & 1;-1 & 1;-1 & 1;-1 \\
\begin{array}{c} \frac{1}{2} \\ \diagdown \end{array} \begin{array}{c} 0 \\ \diagup \end{array} & \begin{array}{c} \frac{1}{2} \\ \diagdown \end{array} \begin{array}{c} 0 \\ \diagup \end{array} & \begin{array}{c} \frac{1}{2} \\ \diagdown \end{array} \begin{array}{c} 0 \\ \diagup \end{array} & \begin{array}{c} \frac{1}{2} \\ \diagdown \end{array} \begin{array}{c} 0 \\ \diagup \end{array} \\
0;0 & 0;0 & 0;0 & 0;0
\end{array} \right) \quad (112)$$

Where in the final equality we write the diagrams as the corresponding matrix with total J values written above the wires and the $J; J_z$ values written horizontal to them.

The connection becomes clearer in the three qubit case showing how the entries of the matrices are the combinations of Clebsch-Gordan coefficients that correspond to particular coupling structures:

$$S_3 = (c_{j_1, m_1; j_2, m_2}^{j_4, m_4} c_{j_4, m_4; j_3, m_3}^{J, M}) = \begin{pmatrix} 1 & 0 & 0 & 0 & 0 & 0 & 0 & 0 \\ 0 & \frac{1}{\sqrt{3}} & \frac{1}{\sqrt{3}} & 0 & \frac{1}{\sqrt{3}} & 0 & 0 & 0 \\ 0 & 0 & 0 & \frac{1}{\sqrt{3}} & 0 & \frac{1}{\sqrt{3}} & \frac{1}{\sqrt{3}} & 0 \\ 0 & 0 & 0 & 0 & 0 & 0 & 0 & 1 \\ 0 & \sqrt{\frac{2}{3}} & -\frac{1}{\sqrt{6}} & 0 & -\frac{1}{\sqrt{6}} & 0 & 0 & 0 \\ 0 & 0 & 0 & -\frac{1}{\sqrt{6}} & 0 & -\frac{1}{\sqrt{6}} & \sqrt{\frac{2}{3}} & 0 \\ 0 & 0 & \frac{1}{\sqrt{2}} & 0 & \frac{1}{\sqrt{2}} & 0 & 0 & 0 \\ 0 & 0 & 0 & -\frac{1}{\sqrt{2}} & 0 & \frac{1}{\sqrt{2}} & 0 & 0 \end{pmatrix} \Leftrightarrow$$



For reasons of space, we merely outline a single diagram with the possible indices highlighted (which is why we don't use equality with the last line). The terms $\frac{1}{2}g1$ and $\frac{1}{2}g0$ serve to separate the two ways one can couple to a total angular momentum of $\frac{1}{2}$ on the last edge. Specifically, $\frac{1}{2}g1$ indicates the case

when the initial coupling resulted in a total angular momentum of 1, and $\frac{1}{2}g0$ is for when it resulted in 0. These have to be distinguished as they correspond to the multiplicities of spin- $\frac{1}{2}$ and so do actually index different elements in the matrix. Here, we merely state the J_z values at the sides of the wires on the RHS and we assume the J_z values range only where permissible.